https://doi.org/10.1016/j.compstruct.2020.113393

Behavior and Modelling of FRP-Concrete-Steel Hybrid Double-Skin Tubular Columns under Repeated Unloading/Reloading Cycles

B. Zhang[1,2], T. Yu[1,*] and J.G. Teng[1]
1. Department of Civil and Environmental Engineering, The Hong Kong Polytechnic University, Hong Kong, China.
2. School of Civil and Environmental Engineering, Harbin Institute of Technology (Shenzhen), Shenzhen, China.

ABSTRACT

Fiber-reinforced polymer (FRP)-concrete-steel hybrid double-skin tubular columns (hybrid DSTCs) consist of an outer FRP tube, an inner steel tube and a concrete infill between the two tubes. Extensive research has been conducted on the monotonic behavior of hybrid DSTCs, but only a limited number of studies have examined their behavior under cyclic axial compression. In particular, no systematic experimental study has been conducted on hybrid DSTCs under repeated unloading/reloading cycles. This paper first presents a systematic experimental study on hybrid DSTCs under two types of loading schemes: (a) a single unloading/reloading cycle to evaluate the relationship between the unloading strain and the plastic strain; (b) repeated unloading/reloading cycles to investigate the effect of loading history. In the present study, hybrid DSTCs were prepared using filament-wound FRP tubes of a relatively large scale (up to 300 mm in diameter), and the experimental program covered a wide range of concrete strengths (from 40.9 MPa to 104.4 MPa). The systematic experimental study with extensive instrumentation allowed the cyclic stress-strain behavior of the concrete in hybrid DSTCs to be examined in detail, clarifying the cumulative effect of the loading history on both the stress deterioration and the plastic strain of the concrete. This paper also presents a detailed comparison between the test results and the predictions of an existing cyclic stress-strain model for FRP-confined concrete in solid columns, in terms of the repeated unloading/reloading cycles. The cyclic stress-strain model is shown to provide reasonably accurate predictions, and thus can be used together with a monotonic stress-stress model for the concrete in hybrid DSTCs to predict the complete cyclic stress-strain curve of such concrete.

Keywords:
Fiber-reinforced polymer (FRP); Double-skin columns; Cyclic loading; Repeated unloading/reloading cycles; High-strength concrete; Confinement.

1 INTRODUCTION

Fiber-reinforced polymer (FRP)-concrete-steel hybrid double-skin tubular columns (hybrid DSTCs) (Figure 1) consist of an outer FRP tube, an inner steel tube and a concrete infill between the two tubes [1, 2]. Because of the use of an FRP tube with excellent corrosion resistance as the external skin, hybrid DSTCs are particularly suitable for use in harsh environments. Hybrid DSTCs are also an attractive column form for seismic regions because of their excellent ductility. In recent years, a large number of studies have been conducted on the monotonic behavior of hybrid DSTCs [1-13], which confirmed the confinement effectiveness provided by the two tubes (i.e. FRP and steel), and the excellent ductility/seismic resistance of these columns.

* Corresponding author; Tel: +852 2766 6042; Email: tao-cee.yu@polyu.edu.hk

The cyclic stress-strain behavior of the concrete in hybrid DSTCs is of particular importance in the modeling of their seismic performance. Yu et al. [14] presented the first-ever study on hybrid DSTCs subjected to cyclic axial compression, in which six specimens (205 mm in diameter and 400 mm in height) made of a wet-layup FRP tube (WL FRP tube) filled with normal strength concrete (NSC) (having an unconfined strength of 43.9 MPa) were tested. Yu et al.'s [14] study confirmed the ductile behavior of hybrid DSTCs with NSC under cyclic axial compression. The effect of loading history on the repeated unloading/reloading cycles was not analyzed in Yu et al. [14] due to the limited number of specimens. Ozbakkaloglu's research group [15-18] reported their cyclic compression tests on small-scale hybrid DSTCs (150 mm in diameter and 300 mm in height) with WL FRP tubes, which demonstrated the ample ductility of the columns even with high strength concrete (HSC) up to 110 MPa. However, these specimens were tested with only one unloading/reloading cycle at each unloading displacement [15-18]. Abdelkarim and ElGawady [19] presented a series of cyclic compression tests on hybrid DSTCs of 210mm in diameter and 406 mm in height; the fibers in the FRP tube of the hybrid DSTCs were oriented at ±45° to the longitudinal axis. Xiong et al. [20] conducted cyclic compression tests on hybrid DSTCs (300 mm in diameter and 600 mm in height) with concrete produced using recycled coarse aggregate. In the tests presented in both Ref. [19] and Ref. [20], three repeated unloading/reloading cycles were executed at each unloading displacement. As the loading history has been shown to have a significant cumulative effect on the behaviour of FRP-confined concrete [21], there is a need to further clarify this effect on the concrete in hybrid DSTCs by cyclic compression tests with more (e.g. >5) repeated unloading/reloading cycles at each unloading displacement.

Against this background, the present paper reports a systematic program of cyclic compression tests on hybrid DSTCs under two types of loading schemes: (a) a single unloading/reloading cycle to evaluate the relationship between the unloading strain and the plastic strain; (b) repeated unloading/reloading cycles (up to 10 repeated cycles) to investigate the effect of loading history. Compared with existing experimental studies, hybrid DSTCs in the present study were designed with special attention to the following three issues that are important in terms of practical applications: the testing of relatively large-scale specimens (up to 300 mm in diameter and 600 mm in height), the use of filament-wound (FW) FRP tubes, and the use of HSC (up to 104.4 MPa). Because of their excellent ductility derived from confinement by the two tubes, hybrid DSTCs provide an ideal opportunity for the use of HSC. For new construction, FW FRP tubes are more suitable for use as the permanent formwork for concrete casting. Extensive strain gauges (up to 5 sections and 20 hoop strain gauges) were attached on the FW FRP tube to evaluate the distribution of hoop rupture strains. The authors [22] has previously proposed a unified cyclic stress-strain model applicable to both NSC and HSC in FRP-confined circular solid section columns. This paper also presents a critical assessment of the applicability of Yu *et al.*'s [22] model to confined NSC/HSC in hybrid DSTCs using the test results of the present study.

2 EXPERIMENTAL PROGRAM

2.1 Specimen Details

A total of 14 hybrid DSTCs were tested under cyclic axial loading as detailed in Table 1. In parallel, 12 corresponding specimens were tested under monotonic loading and their results were presented in Zhang *et al.* [23]. For ease of comparison, the key

information of the 12 monotonically loaded specimens is also summarized in Table 1.

The specimens were fabricated in six batches with six different concrete strengths (from 40.9 MPa to 104.4 MPa). These specimens mainly had two sizes: (1) 200 mm in diameter and 400 mm in height (specimens of batches 1-3); (2) 300 mm in diameter and 600 mm in height (specimens of batches 4-6). Glass FRP tubes which were manufactured via a filament-winding process were employed. In these FRP tubes, the fibers were orientated at ± 80 degrees to the longitudinal axis. In hybrid DSTCs, the FRP tube serves as a corrosion-resistant protective skin, a stay-in-place form, and a confining device for the concrete inside. Due to its functions, the FRP tube should have fibres close to the hoop direction of the tube (e.g. ± 80 degrees to the longitudinal axis as those used in the tests presented in this paper) [2]. In Table 1, the void ratio φ is defined as the ratio of the inner diameter D_s to the outer diameter D of the concrete section of a DSTC; t_s and t_{frp} are the thicknesses of the steel tube and the FRP tube, respectively. The present study covered three void ratios (i.e., 0.600, 0.730 and 0.795) and three types of steel tubes (i.e. types A, B and C) (Tables 1 and 2).

Each specimen is given a name which has four components in sequence: (1) a letter "D" to represent "DSTC", followed by a number to represent the unconfined concrete strength (in MPa); (2) a one-digit number to indicate the thickness (in mm) of the FRP tube, together with two letters "FW" to represent filament-wound FRP tubes; (3) a letter "C" or "M" to represent cyclic or monotonic axial compression; (4) a number "1" or 2" in some names to differentiate two nominally identical specimens. The steel tube type is not reflected in the name, except for the specimens with a steel tube of type B (e.g., specimen D84-4FW-CB); the names of these specimens have an additional letter "B" at the end. Typical cross-sections of hybrid DSTCs are shown in Figure 2.

2.2 Material Properties

2.2.1 Concrete

In the test specimens of hybrid DSTCs, the annular concrete layer between the inner steel tube and the outer FRP tube had a small thickness. To ensure the quality of concrete casting, self-compacting concrete was adopted instead of regular concrete. Table 3 summarizes the mix proportions of the concrete. Three standard concrete cylinders (152.5 mm in diameter and 305 mm in height) were prepared and tested for each batch of concrete to obtain their mechanical properties following ASTM C39/C39M [24]. Strain gauges with a gauge length of 100 mm were attached on the concrete cylinder to obtain the axial strains. The key test results, including the elastic modulus E_c, cylinder compressive strength f'_{co} and the corresponding strain ε_{co}, are summarized in Table 4.

2.2.2 FRP Tubes

Five types of FW FRP tubes were used, which were nominally the same as those used in the corresponding DSTCs tested under monotonic loading (see Zhang *et al*. [23]). Tensile split-disk tests and compression tests of these FRP tubes were conducted. The details of the tests are presented in Zhang *et al*. [23] and are summarized below for ease of reference.

Tensile split-disk tests were carried out in accordance with ASTM D2290-08 [25] to obtain the hoop tensile properties of FRP tubes. All the FW FRP tubes with the same diameter (i.e. 200 mm or 300 mm) had the same orientations of fibers and the same

nominal volume ratio, so tests were only conducted on one selected type of tubes for each diameter. The average secant elastic modulus, hoop stress, and hoop strain at failure obtained from five FRP rings of each type were 45.9 GPa, 659.1 MPa and 1.49%, respectively, for the 200 mm tubes, while the results were 43.6 GPa, 663.7 MPa and 1.55%, respectively, for the 300 mm tubes.

Compression tests were conducted following the Chinese Standard GB/T5350 [26] to obtain the axial compressive properties of FRP tubes. Only FRP rings from a selected tube with a diameter of 200 mm were tested, and it was found that the average secant elastic modulus, axial stress and axial strain at failure were 10.0 GPa, 95.1 MPa and 0.95%, respectively. The 300 mm tubes had fibers oriented in directions which were the same as those of the 200 mm tubes, so their compressive stress-strain curves in the longitudinal direction are assumed to be the same as those of the 200 mm tubes.

2.2.3 Steel Tubes

For each type of steel tubes, the elastic modulus E_s, the yield stress f_y and the ultimate stress f_u were obtained from three tensile coupon tests following BS 18 [27]. Table 2 summarizes the test results. In addition, monotonic compression tests were conducted on two hollow steel tubes of each type, while another tube of each type was tested under cyclic compression. The heights of the hollow tubes were the same as those used in the corresponding hybrid DSTCs. It is known that the use of shorter tubes reduces the likelihood of global buckling of the hollow steel tube. The hollow steel tubes tested in the present study all failed by local buckling in the elephant-foot mode, so the effect of the tube height on their axial compressive behavior is believed to be small. The axial stress-axial strain curves of these specimens are shown in Figure 3, where the axial strains were calculated from the overall shortenings of the specimen. It is evident that the slopes of the unloading/reloading paths of the cyclic stress-strain curves are almost the same as the initial elastic modulus of the steel.

2.3 Experimental Setup and Instrumentation

A large testing facility with an axial compression capacity of 10,000 kN was used to conduct the axial compression tests (Figure 4). For each specimen of the first three batches, four LVDTs (LVDT-400) were installed to obtain the axial shortening (Figure 5a). At the same time, four axial strain gauges with a 20 mm gauge length (i.e. SG-20) and four axial strain gauges with a 100 mm gauge length (i.e. SG-100) were attached on the outer surface of each FRP tube at the mid-height section. The hoop strains were measured by a large number of strain gauges (of a 20 mm gauge length) at three different sections of each FRP tube: mid-height, 100 mm below and 100 mm above than the mid-height; at each section, four strain gauges were evenly distributed around the circumference. In addition, two 10 mm strain rosettes were attached on the internal surface of the steel tube to monitor the strain state at its mid-height.

For each specimen of batches 4-6 (Figure 5b), four LVDTs (i.e. LVDT-320) were installed to measure the axial deformation of the 320 mm mid-height region, while another four (i.e. LVDT-600) were installed to obtain the total axial shortening. Eight axial strain gauges, which were the same as those for the specimens of batches 1-3, were installed at the mid-height of the FRP tube. Hoop strains at five different heights of the FRP tube were measured: mid-height, 80 mm and 160 mm below the mid-height, 80 mm and 160 mm above the mid-height. Eight hoop strain gauges were installed at the mid-height section, while four hoop strain gauges were installed at each of the other

heights. Again, the strain state of the inner steel tube was monitored by two 10 mm strain rosettes at its mid-height.

2.4 Loading Schemes

All compression tests were conducted with displacement control (0.24 mm/min for the specimens of batches 1-3, and 0.36 mm/min for those of batches 4-6). The axial load was applied on all components of the specimen (i.e. FRP tube, concrete and steel tube) simultaneously. The cyclic loading schemes were executed using the displacement readings averaged from the LVDTs (i.e. LVDT-400 for specimens of batches 1-3; LVDT-600 for specimens of batches 4-6) and the load readings from the column testing facility as the controlling parameters.

In order to investigate the effect of loading history, two cyclic loading schemes were adopted: (1) type C1: a single unloading/reloading cycle at a prescribed unloading displacement value; (2) type C2: several repeated unloading/reloading cycles at a prescribed unloading displacement value. Both types of loading schemes employed the so-called full unloading/reloading cycles, where the unloading was terminated at zero force and the reloading was terminated when the unloading displacement of the same cycle was reached [28]. For the specimens of batches 1-3, they were each subjected to a combination of type C1 and C2 loading: type C1 loading for the first few prescribed unloading displacement values, followed by type C2 loading involving 10 repeated cycles at the final prescribed unloading displacement value. For specimen D84-4FW-CB, only three of the 10 intended repeated cycles were finished before the failure of the specimen. For the groups in batches 4-6 with two nominally identical, cyclically loaded specimens for each sectional configuration (i.e. D40-6FW, D66-6FW, D85-6FW), one was tested under type C1 loading while the other was tested under type C2 loading. For specimen D85-10FW-C, type C1 loading was adopted. Table 5 summarizes the details of the loading schemes.

3 TEST OBSERVATIONS

3.1 General

The failure process of cyclically loaded hybrid DSTCs is similar to that of the monotonically loaded hybrid DSTCs as presented in Zhang *et al*. [23]. The failure of the FRP tube started with the progressive snapping of fibers, and ended with the explosive rupture of the tube with a big noise. Axial load fluctuations and/or a sudden load drop were observed for cyclically loaded hybrid DSTCs with HSC (Figure 8), which is similar to the observation made by Zhang *et al*. [23] about the monotonically loaded specimens.

After the tests, the specimens were carefully examined. Damages to the FRP tube, the concrete and the inner steel tube are shown for typical specimens in Figure 6. As expected, damage localization was found in all specimens. The rupture of FRP tube occurred at or close to locations where the concrete experienced severe damage while the steel tube experienced inward deformation/buckling.

3.2 Axial Strains

Both axial strain gauges and LVDTs were used to measure the axial deformation of the specimens, which provided several ways to obtain the axial strains of the specimen. The average strain of the whole specimen, which was calculated using readings from four LVDTs (i.e. LVDTs-400 for specimens of batches 1-3; LVDTs-600 for specimens of

batches 4-6), is referred to as the nominal axial strain. Similar to the discussions in Zhang *et al*. [23], the nominal axial strain generally agrees well with strain gauge readings before the strain value reaches around 0.005; after that the former becomes significantly larger than the latter. For specimens in batches 4-6, four LVDTs (i.e. LVDTs-320) were also installed to measure the deformation of the 320 mm mid-height region. The nominal axial strain was found to be close to the strain calculated from the LVDT-320 readings, except for the specimens which experienced local damage outside the 320 mm mid-height region. It is evident that after significant local damage of concrete, the readings of LVDT-320 or axial strain gauges may not closely reflect the strain state of the confined concrete. The nominal axial strain is thus used to represent the axial strain of concrete, unless otherwise specified. Readers may refer to Zhang *et al*. [23] for detailed discussions of the axial strains.

3.3 Hoop Strains

Many strain gauges were attached on the FW FRP tube to measure the hoop strains at different locations. The distributions of hoop strains are shown in Figure 7 for the ultimate state of all the specimens.

It is evident in Figure 7 that the hoop rupture strain of cyclically loaded specimens is generally smaller than that of the corresponding monotonically loaded specimens, which is believed to be due to the accumulation of localized damage in the FRP tube caused by cyclic straining. In addition, the following observations, which are similar to those reported by Zhang *et al*. [23] for monotonically loaded specimens, can be made: (1) the maximum and minimum hoop strains generally occurred not at the mid-height; (2) while the hoop strain readings are quite scattered, the average of all the readings ($\varepsilon_{h,rup1}$) is close to the average reading at the mid-height section ($\varepsilon_{h,rup2}$); (3) the average hoop rupture strain is relatively small for the specimens with HSC and/or a weak FRP tube.

4 BEHAVIOR OF CONFINED CONCRETE

4.1 Axial Load-Axial Strain Curves of Hybrid DSTCs

Axial load-axial strain curves of cyclically loaded hybrid DSTCs are compared with those of their monotonically loaded counterparts in Figure 8. It is evident that the envelope curves of all the cyclically loaded specimens coincide well with the corresponding monotonic curves. This observation is consistent with that reported for hybrid DSTCs with a WL FRP tube [14, 16, 17].

4.2 Axial Stress-Axial Strain Behavior of Concrete

In hybrid DSTCs, the axial load is taken by the confined concrete, the steel tube as well as the FRP tube. Similar to Zhang *et al*. [23], in the present study, the load taken by the concrete section is assumed to be equal to the overall load carried by the specimen subtracted by those taken by the FRP tube and the steel tube at the same axial strain, while the axial stress of the concrete is calculated by dividing the load it takes by its cross-sectional area.

Similar to Zhang *et al*. [23], the load taken by the FRP tube under monotonic loading is found from compression tests on hollow FRP tubes, assuming that the load taken by FRP is equal to its ultimate load when the axial strain exceeds the ultimate strain from the hollow FRP tube tests. For the load taken by the FRP tube subjected to unloading/reloading cycles, it is assumed that the load taken by the FRP tube decreases

(or increases) proportionally to the total axial load taken by the specimen. This assumption is believed to cause only marginal errors considering the small axial stiffness and small cross-sectional area of the FRP tube.

To find the load taken by the inner steel tube during cyclic loading is more involved. Yu *et al.* [14] found that the plastic strain of the steel tube is generally larger than that of the concrete, and the axial strain at zero force of the specimen is generally between the two. This means that tensile stresses may be developed in the steel tube during the unloading process of hybrid DSTCs, with balancing compressive stresses in the concrete. The bond/friction between the steel tube and the concrete ensures force equilibrium to be reached. In the present study, both monotonic and cyclic axial compression tests on hollow steel tubes were conducted, but the behavior of steel tubes under reversed cyclic axial loading was not tested due to the limitation of testing machine.

Many models have been proposed for the reversed cyclic stress-strain relationship of steel, and they mainly fall into two types: (a) Ramberg-Osgood type model [29]; and (b) Guiffre-Menegotto-Pinto type model [30]. In the present study, the Ramberg-Osgood type model proposed by Yokoo and Nakamura [31], which was found to be accurate yet simple [32], was adopted to find the load taken by the inner steel tube from the experimental axial strain readings. Yokoo and Nakamura's [31] model can be expressed by the following equation:

$$\varepsilon_s - \varepsilon_i = \frac{f_s - f_i}{E_s}\left[1 + A^{-R}\left|\frac{f_s - f_i}{f_y}\right|^{R-1}\right] \quad (1)$$

where: f_s and ε_s are the stress and strain of cyclically loaded steel, respectively; f_i and ε_i are the stress and strain of cyclically loaded steel at the load reversal point, respectively; E_s is the Young's modulus of steel; f_y is the yield stress of steel; $A = 1.9k_p^{-0.2}$ and $R = 10k_p^{-0.2}$; k_p is the plastic strain ratio, which is defined as $\varepsilon_p/\varepsilon_n = (\varepsilon_i - \varepsilon_n)/\varepsilon_n$. Here, ε_n is the initial yield strain, and ε_p is the plastic strain. Readers may refer to Yokoo and Nakamura [31] and Mansour *et al*. [32] for more details of this model.

Figure 9 shows the cyclic stress-strain curves of confined concrete in two of the tested hybrid DSTCs (i.e. specimens D40-6FW-C2 and D85-10FW-C) obtained by using Eq. 1 and the average axial strains obtained from the two axial strain gauges on the inner steel tube. Figure 9 shows that for the first two prescribed unloading strains which were smaller than 0.005, the concrete stress reached zero when the specimens were unloaded to zero load. However, for the larger unloading strains, compressive stresses in the concrete, and thus tensile stresses in the steel existed when the overall load taken by the specimen became zero. It is also interesting to note that the concrete stresses at the zero overall load point are almost identical for different unloading strains (all being larger than 0.005), which is probably due to the limit of bond strength between the steel tube and the concrete.

As explained above, readings from the axial strain gauges on the steel tube need to be used to deduce the axial stress-strain curves of concrete. However, in all the specimens except specimens D40-6FW-C2 and D85-10FW-C, the strain gauges stopped functioning before the end of the test due to the localized damage of concrete and steel. Typically these strain readings were only available for the first 4-6 prescribed

unloading/reloading cycles. For these specimens, the following methodology was adopted to obtain the load taken by the steel tube:

(a) For unloading/reloading cycles where the axial strain readings of the steel tube were available, Eq. 1 was used together with these strain readings;
(b) For other cycles, based on the observation from Figure 9, it was assumed that the tensile stresses of steel at the zero overall load point were all equal to a constant value; this constant value was found following step (a) using the average stress of steel at zero overall load from the few cycles at unloading strains larger than 0.005 of the same specimen;
(c) it was further assumed that the load taken by the steel tube changed proportionally to the overall axial load taken by the specimen, with the steel reaching a tensile load corresponding to the tensile stress found from step (b) when the overall load became zero.

Figure 9 shows a comparison between the stress-strain curves of concrete obtained using the assumptions listed above and those found using Eq. 1 for the two hybrid DSTC specimens (i.e., specimens D40-6FW-C2 and D85-10FW-C) whose strain gauges on the steel tube remained functioning until the end of test. A very good agreement is seen for both specimens in Figure 9, which demonstrates the validity of the proposed assumptions.

The axial stress-strain curves of the confined concrete in hybrid DSTCs obtained with the above assumptions are shown in Figure 10 for both cyclically loaded and monotonically loaded specimens. As demonstrated in Figure 10, the concrete in hybrid DSTCs possesses the following key characteristics: (1) the envelope curve generally coincides with the monotonic stress-strain curve; (2) the loading history has a cumulative effect on both the stress deterioration and plastic strain; (3) the unloading path is significantly nonlinear while the reloading path is almost linear. These characteristics are similar to those of FRP-confined concrete in a solid column (Yu *et al*. 2015).

4.3 Key Results

Table 6 summarizes the key test results of all hybrid DSTCs. In Table 6, F_{all} is the peak axial load taken by the whole specimen; F_c is the peak axial load resisted by the concrete; $f_{cc}^{'}$ is the peak axial stress of the concrete; ε_{cu} is the ultimate axial strain of the concrete when the FRP tube ruptures; $f_{co}^{'}$ and ε_{co} are the peak axial stress and the strain at the peak axial stress of unconfined concrete, respectively.

5 CYCLIC AXIAL STRESS-STRAIN MODEL

5.1 General

The authors [22] proposed a unified cyclic stress-strain model for NSC and HSC confined by FRP, which was developed based on a test database of FRP-confined solid concrete columns [15, 33-37]. Yu *et al*.'s [22] model is a revised version of the model proposed by Lam and Teng [28], and provides a set of equations to depict the cyclic stress-strain curves (Figure 11). Some of the equations of Yu *et al*.'s [22] model are provided below wherever necessary, while readers may refer to Yu *et al* [22] for details of the model.

Considering the similarity between the concrete in hybrid DSTCs and that in FRP-confined solid columns, as discussed in section 4.2, it is not unreasonable to expect that the same model may work for both cases. In the following subsections, the applicability of Yu *et al.*'s [22] model to hybrid DSTCs with NSC/ HSC is critically assessed in terms of the unloading path, stress deterioration and plastic strain of the envelope curve, effects of loading history (i.e., on the plastic strain recovery ratio and stress deterioration ratio of internal cycles), and the overall performance of unloading/reloading cycles.

5.2 Unloading Path

In Yu *et al.*'s [22] model, the unloading path is predicted by Eqs. 2-6, in which the effect of unconfined concrete strength f'_{co} is considered:

$$\sigma_c = a\varepsilon_c^{\eta} + b\varepsilon_c + c \tag{2}$$

$$a = \frac{\sigma_{un} - E_{un,0}(\varepsilon_{un} - \varepsilon_{pl})}{\varepsilon_{un}^{\eta} - \varepsilon_{pl}^{\eta} - \eta\varepsilon_{pl}^{\eta-1}(\varepsilon_{un} - \varepsilon_{pl})} \tag{3}$$

$$b = E_{un,0} - \eta\varepsilon_{pl}^{\eta-1}a \tag{4}$$

$$c = -a\varepsilon_{pl}^{\eta} - b\varepsilon_{pl} \tag{5}$$

$$\eta = 40(350\varepsilon_{un} + 3)/f'_{co} \tag{6}$$

where: σ_c and ε_c are the axial stress and axial strain of concrete respectively; $E_{un,0}$ is the slope of the unloading path at zero stress; η is a coefficient which is dependent on the unconfined concrete strength f'_{co} and the unloading strain ε_{un}; a, b, and c are the three coefficients for Eq. 2 which are determined by the unloading strain ε_{un}, the plastic strain ε_{pl}, the slope of the unloading path at zero stress $E_{un,0}$ and the coefficient η.

Eqs. 2-6 are used here to predict the unloading curves of concrete in hybrid DSTCs as shown in Figure 12. In doing so, the experimental unloading strain ε_{un}, experimental unloading stress σ_{un} and experimental plastic strain ε_{pl} were used. Therefore, the comparison shown in Figure 12 reflects only the performance of the equations for the unloading path (i.e. Eqs. 2-6). As the compressive stresses of the confined concrete at the termination point of unloading path were not zero (Figure 12), the plastic strain values ε_{pl} were evaluated by extending the unloading path of the experimental stress-strain curve smoothly to the zero stress point, as suggested by Lam *et al.* [35]. Figure 12 shows that Yu *et al.*'s [22] equations for the unloading path (i.e. Eqs. 2-6) provide accurate predictions for the concrete in hybrid DSTCs.

5.3 Plastic Strain of an Envelope Cycle

In Lam and Teng [28], the equation for predicting the plastic strain of an envelope unloading curve $\varepsilon_{pl,1}$ of FRP-confined concrete has two controlling parameters, which are the unconfined concrete strength f'_{co} and the envelope unloading strain $\varepsilon_{un,env}$. The new test data [15, 21] indicated that the unconfined concrete strength f'_{co} has no significant effect on the envelope plastic strain $\varepsilon_{pl,1}$. In Yu *et al.*'s [22] model, the following equation was proposed for predicting the plastic strain of envelope, in which the unconfined concrete strength f'_{co} was excluded as a parameter:

$$\varepsilon_{pl,1} = \begin{cases} 0 & 0 < \varepsilon_{un,env} \le 0.001 \\ 0.184\varepsilon_{un,env} - 0.0002 & 0.001 < \varepsilon_{un,env} \le 0.0035 \\ 0.703\varepsilon_{un,env} - 0.002 & 0.0035 < \varepsilon_{un,env} \le \varepsilon_{cu} \end{cases} \tag{7}$$

For the concrete in hybrid DSTCs under cyclic compression, the envelope plastic strains $\varepsilon_{pl,1}$ are shown against the envelope unloading strains $\varepsilon_{un,env}$ in Figure 13. It is evident from Figure 13 that there is a linear relationship between $\varepsilon_{pl,1}$ and $\varepsilon_{un,env}$ when the latter is larger than 0.0035; this observation is consistent with Eq. 7. To further examine this issue, regression analysis was conducted for the data points of each hybrid DSTC in the present study (for $0.0035 < \varepsilon_{un,env} \leq \varepsilon_{cu}$), and the statistical characteristics of the linear trend lines are summarized in Table 7. Similar to FRP-confined concrete [22], this linear relationship appears to be not considerably affected by f'_{co}. The coefficient *a* in Table 7 (i.e. the slope of the trend line) is further shown against f'_{co} in Figure 14, which clearly indicates that *a* is almost the same for most hybrid DSTCs despite the variation of unconfined concrete strength (i.e. from 40.1 MPa to 104.4 MPa).

By averaging the *a* and *b* (i.e. the y-intercept of the trendline) values of all specimens in Table 7, the third sub-equation (for $0.0035 < \varepsilon_{un,env} \leq \varepsilon_{cu}$) of Eq. 7 can be revised. By doing so, the second sub-equation (for $0.001 < \varepsilon_{un,env} \leq 0.0035$) needs to be revised correspondingly to ensure the continuity of $\varepsilon_{pl,1}$. The following equations are thus obtained for the envelope plastic strain $\varepsilon_{pl,1}$, without using f'_{co} as a parameter:

$$\varepsilon_{pl,1} = \begin{cases} 0 & 0 < \varepsilon_{un,env} \leq 0.001 \\ 0.292\varepsilon_{un,env} - 0.0003 & 0.001 < \varepsilon_{un,env} \leq 0.0035 \\ 0.781\varepsilon_{un,env} - 0.003 & 0.0035 < \varepsilon_{un,env} \leq \varepsilon_{cu} \end{cases} \quad (8)$$

It is seen in Figure 15 that Eq. 8 is able to predict the test results reasonably accurately. For comparison, the predictions of Eq. 7, which were developed based on a large amount of test data of cyclically loaded FRP-confined concrete, are also shown against the experimental results of hybrid DSTCs in Figure 15. It is interesting to note that Eq. 7 also provides reasonably accurate predictions of $\varepsilon_{pl,1}$ for hybrid DSTCs, although its performance is slightly worse than Eq. 8. Considering the scatter of experimental results and the possible errors that might have been caused by the methodology for obtaining the experimental stress-strain curves, it is reasonable to suggest that Eq. 7 is also applicable to the confined concrete in hybrid DSTCs.

5.4 Stress Deterioration of Envelope Cycles

In Yu *et al.*'s [22] model, the new stress $\sigma_{new,1}$ on the first reloading path at the envelope unloading strain is calculated as the product of the envelope unloading stress $\sigma_{un,env}$ and the stress deterioration ratio ϕ_1 of envelope cycles, which is determined by the following equation:

$$\phi_1 = \frac{\sigma_{new,1}}{\sigma_{un,env}} = \begin{cases} 1 & 0 < \varepsilon_{un,env} \leq 0.001 \\ 1 - 32(\varepsilon_{un,env} - 0.001) & 0.001 < \varepsilon_{un,env} \leq 0.0035 \\ 0.92 & 0.0035 < \varepsilon_{un,env} \leq \varepsilon_{cu} \end{cases} \quad (9)$$

Figure 16 shows a comparison between the predictions of Eq. 9 and the test results of the confined concrete in hybrid DSTCs, and demonstrates that Eq. 9 can be directly adopted for hybrid DSTCs.

5.5 Effect of Loading History

It is evident that the loading history (i.e. repeated unloading/reloading cycles) has a

cumulative effect on both stress deterioration and the plastic strain of the concrete in hybrid DSTCs (Figure 10). Equations for the cumulative effects of loading history are given in Lam and Teng [28], which were based on limited test results with the maximum number of full unloading/reloading cycles being three. Yu *et al*. [22] modified these equations on the basis of a larger test database with the maximum number of full unloading/reloading cycles being 12.

In Yu *et al*.'s [22] model, two factors are adopted to define the effects of loading history: the strain recovery ratio ω_n which defines the accumulation of plastic strain with the number of repeated cycles, and the stress deterioration ratio ϕ_n which defines the cumulative effect of repeated cycles on stress deterioration. For full unloading/reloading cycles, ω_n $(n \geq 2)$ and ϕ_n are defined by the following two equations, respectively:

$$\omega_n = \frac{\varepsilon_{un,n} - \varepsilon_{pl,n}}{\varepsilon_{un,n} - \varepsilon_{pl,n-1}} = \begin{cases} 1 & 0 < \varepsilon_{un,env} \leq 0.001 \\ 1 - 32(\varepsilon_{un,env} - 0.001)/(n-1) & 0.001 < \varepsilon_{un,env} \leq 0.0035 \\ -0.08/(n-1) + 1 & 0.0035 < \varepsilon_{un,env} \leq \varepsilon_{cu} \end{cases} \quad (10)$$

$$\phi_n = \frac{\sigma_{new,n}}{\sigma_{ref,n}} = \begin{cases} 1 & 0 < \varepsilon_{un,env} \leq 0.001 \\ 1 - 80(\varepsilon_{un,env} - 0.001)/n & 0.001 < \varepsilon_{un,env} \leq 0.002 \\ -0.08/n + 1 & 0.002 < \varepsilon_{un,env} \leq \varepsilon_{cu} \end{cases} \quad (11)$$

where: n is the counting number of the current full unloading/reloading cycle; ω_n is the strain recovery ratio for the n^{th} full unloading/reloading cycle; ϕ_n is the stress deterioration ratio for the n^{th} full unloading/reloading cycle; $\varepsilon_{un,n}$, $\varepsilon_{ref,n}$and $\varepsilon_{pl,n}$ are the unloading strain, the reference strain and the plastic strain for the n^{th} full unloading/reloading cycle, respectively; $\sigma_{un,n}$, $\sigma_{new,n}$ and $\sigma_{ref,n}$ are the unloading stress, the new stress and the reference stress for the n^{th} full unloading/reloading cycle, respectively; $\sigma_{un,n} = \sigma_{new,n-1}$ and $\varepsilon_{un,n} = \varepsilon_{ref,n-1}$ for full unloading/reloading cycles in the present study.

It should be noted that in the experiments presented in this paper, although unloading was terminated at zero force, the stress of concrete was not exactly zero at the termination point (Figure 10). Therefore, these unloading paths are not perfectly "full unloading paths" according to the definition of Yu *et al* [22]. Nevertheless, as the concrete stress was typically small at the termination point of unloading, Eqs. 10 and 11 were used to predict the test results in the present study. This simplification is believed to have led to only a marginal difference in the predictions.

Figures 17 and 18 shows that Yu *et al*.'s [22] equations for predicting the plastic strain recovery ratio (i.e. Eq. 10) and the stress deterioration ratio (i.e. Eq. 11) of internal cycles can also yield accurate predictions for the mean experimental values for the concrete in hybrid DSTCs, and thus can be directly used for hybrid DSTCs.

5.6 Overall Performance for Unloading/Reloading Cycles

The overall performance of the Yu *et al*.'s [22] model is evaluated in Figures 19 and 20 in terms of the envelope unloading/reloading curves and the repeated unloading/reloading curves, respectively.

In making the predictions given in Figure 19, the experimental strain $\varepsilon_{un,env}$ and stress $\sigma_{un,env}$ on the envelope curve were used as the starting point of the prediction. It is evident from Figure 19 that Yu *et al*.'s [22] model can provide reasonably accurate

predictions for the envelope unloading/reloading curves of the confined concrete in hybrid DSTCs.

In making the predictions given in Figure 20, the experimental strain $\varepsilon_{un,env}$ and stress $\sigma_{un,env}$ on the envelope curve as well as the experimental plastic strain of envelope curve $\varepsilon_{pl,1}$ were used. Each experimental cycle is shown against the prediction separately. Typical comparisons (for the 1st, 4th, 7th and 10th cycles) are shown in Figure 20 for specimens in batches 1-3, while the comparisons for other cycles are generally similar. Again, Yu *et al.*'s [22] model is seen to capture the plastic strain and the stress deterioration of the confined concrete with reasonable accuracy, and can yield reasonably accurate predictions for repeated unloading/reloading curves of the concrete in hybrid DSTCs.

5.7 Remarks

It is evident from the above discussions that Yu *et al.*'s [22] model can provide reasonably accurate predictions for the unloading/reloading paths and the effects of loading history for the concrete in hybrid DSTCs. However, in the above discussions, the test results of stresses/strains on the envelop curves are adopted. It should be noted that Yu *et al.*'s [22] model was proposed for the concrete in FRP-confined solid columns, so the equations in their model for the envelope curve cannot be directly applied to the concrete in hybrid DSTCs whose behavior depends also on the void ratio of the DSTCs [5]. To provide a complete prediction of the cyclic stress-strain behaviour of the concrete in hybrid DSTCs, Yu *et al.*'s [22] model should be used together with a monotonic stress-strain model specially developed for the concrete in hybrid DSTCs [5] .

It should also be noted that Yu *et al.*'s [22] model includes equations for the cases of partial unloading/reloading cycles, where unloading is terminated at a stress considerably larger than zero and/or the reloading is terminated before reaching the reference strain. These equations are not validated due to the lack of test results, but are herein recommended to be used before further research on these issues becomes available.

6 CONCLUSIONS

This paper has presented the results of cyclic axial compression tests on hybrid DSTCs under two loading schemes: (a) a single unloading/reloading cycle; (b) repeated unloading/reloading cycles (up to 10 repeated cycles). The following conclusions can be drawn based on the results and discussions presented in the paper:

(1) The envelope stress-strain curve of concrete in a cyclically loaded hybrid DSTC is nearly the same as the stress-strain curve of concrete in the corresponding monotonically loaded specimen;
(2) The hoop rupture strain (either $\varepsilon_{h,rup1}$ or $\varepsilon_{h,rup2}$) of a cyclically loaded specimen is generally smaller than that of the corresponding monotonically loaded specimen, which is believed to be due to damage accumulation in the FRP tube caused by cyclic straining;
(3) The characteristics of unloading/reloading behavior of confined concrete in cyclically loaded hybrid DSTCs are generally similar to those of confined concrete in FRP-confined solid concrete columns;
(4) The loading history (i.e. repeated unloading/reloading cycles) has a cumulative

effect on both stress deterioration and the plastic strain of concrete in hybrid DSTCs;

(5) The part of Yu *et al*.'s [22] model for unloading/reloading cycles can be used together with a monotonic stress-strain model for the concrete in hybrid DSTCs to provide accurate predictions of the cyclic stress-strain response of such concrete.

ACKNOWLEDGMENT

The authors are grateful for the financial support received from the National Key R&D Program of China (Project No. 2017YFC0703000) and the National Natural Science Foundation of China (Grant No. 51978332, 51608263).

REFERENCES

[1] Teng, J.G., Yu, T. and Wong, Y.L. (2004). "Behaviour of hybrid FRP-concrete-steel double-skin tubular columns", *Proceedings, Second International Conference on FRP Composites in Civil Engineering*, 8-10 December, Adelaide, Australia, 811-818.

[2] Teng, J.G., Yu, T., Wong, Y.L. and Dong, S.L. (2007). "Hybrid FRP-concrete-steel tubular columns: Concept and behavior", *Construction and Building Materials*, 21(4), 846-854.

[3] Yu, T. (2007). *Behavior of Hybrid FRP-Concrete-Steel Double-Skin Tubular Columns*, PhD Thesis, The Hong Kong Polytechnic University.

[4] Wong, Y.L., Yu, T., Teng, J.G. and Dong, S.L. (2008). "Behavior of FRP confined concrete in annular section columns", *Composites Part B: Engineering*, 39(3), 451-466.

[5] Yu, T., Teng, J.G. and Wong, Y.L. (2010). "Stress-strain behavior of concrete in hybrid double-skin tubular columns", *Journal of Structural Engineering*, ASCE, 136(4), 379-389.

[6] Zhang, B., Yu, T. and Teng, J.G. (2011). "Axial compression tests on hybrid double-skin tubular columns filled with high strength concrete", *Proceedings, Third International Postgraduate Conference on Infrastructure and Environment*, 11-12 July, Hong Kong, China, 171-176.

[7] Xie, P., Yu, T., Wong, Y.L. and Teng, J.G. (2011). "Compressive behavior of large-scale hybrid FRP-concrete-steel double-skin tubular columns", *Advanced Materials Research*, 243, 1138-1144.

[8] Yu, T. and Teng, J.G. (2013). "Behavior of hybrid FRP-concrete-steel double-skin tubular columns with a square outer tube and a circular inner tube subjected to axial compression", *Journal of Composites for Construction*, ASCE, 17(2), 271-279.

[9] Ozbakkaloglu, T. and Louk Fanggi, B.A. (2014). "Axial compressive behavior of FRP-concrete-steel double-skin tubular columns made of normal-and high-strength concrete", *Journal of Composites for Construction*, ASCE, 18(1) 04013027.

[10] Louk Fanggi, B.A. and Ozbakkaloglu. T. (2013). "Compressive behavior of aramid FRP-HSC-steel double-skin tubular columns", *Construction and Building Materials*, 48(0), 554-565.

[11] Louk Fanggi, B.A. and Ozbakkaloglu. T. (2015). "Behavior of hollow and concrete-filled FRP-HSC and FRP-HSC-steel composite columns subjected to concentric compression", *Advances in Structural Engineering*, 18(5), 715-738.

[12] Louk Fanggi, B.A. and Ozbakkaloglu. T. (2015). "Square FRP-HSC-steel composite columns: Behavior under axial compression", *Engineering Structures*, 92, 156-171.

[13] Zhang, B., Zhao, J.L., Huang, T., Zhang, N.Y., Zhang, Y.J., and Hu, X.M. (2020) "Effect of fiber angles on hybrid FRP-concrete-steel double-skin tubular columns under monotonic axial compression", *Advances in Structural Engineering*, https://doi.org/10.1177/1369433219895916.

[14] Yu, T., Zhang, B., Cao, Y.B. and Teng, J.G. (2012). "Behavior of hybrid FRP-concrete-steel double-skin tubular columns subjected to cyclic axial compression", *Thin-Walled Structures*, 61, 196-203.

[15] Ozbakkaloglu, T. and Akin, E. (2012) "Behavior of FRP-confined normal-and high-strength concrete under cyclic axial compression", *Journal of Composites for Construction*, ASCE, 16, 451-463.

[16] Louk Fanggi, B.A. and Ozbakkaloglu. T. (2014). "Influence of concrete and FRP tubes properties on behavior of FRP-concrete-steel double-skin tubular columns subjected to cyclic axial compression", Proceedings, *13th International Symposiums on Structural Engineering (ISSE)*, Hefei, China, 572-580.

[17] Ozbakkaloglu, T. and Louk Fanggi, B.A. (2015). "FRP-HSC-steel composite columns: behavior under monotonic and cyclic axial compression", *Materials and Structures*, 48, 1075-1093.

[18] Albitar, M., Ozbakkaloglu, T. and Louk Fanggi, B.A. (2015). "Behavior of FRP-HSC-Steel Double-Skin Tubular Columns under Cyclic Axial Compression", *Journal of Composites for Construction*, ASCE, 19(2), 04014041.

[19] Abdelkarim, O.I. and ElGawady, M.A. (2016). "Behavior of hollow FRP-concrete-steel columns under static cyclic axial compressive loading", *Engineering Structures*, 123, 77-88.

[20] Xiong, Z., Cai, Q.L., Liu, F., Li, L.J. and Long, Y.L. (2020). "Dynamic performance of RAC-filled double-skin tubular columns subjected to cyclic axial compression", *Construction and Building Materials*, 248, DOI: 10.1016/j.conbuildmat.2020.118665.

[21] Zhang, B., Yu, T. and Teng, J.G. (2015). "Behaviour of concrete-filled FRP tubes under cyclic axial compression", *Journal of Composites for Construction*, ASCE, Journal of Composites for Construction 19 (3), 04014060.
[22] Yu, T., Zhang, B. and Teng, J.G. (2015). "Unified stress-strain model for FRP-confined concrete under cyclic axial compression", *Engineering Structures*, 102, 189-201.
[23] Zhang, B., Teng, J.G. and Yu, T. (2017). "Compressive Behavior of Double-Skin Tubular Columns with High-Strength Concrete and a Filament-Wound FRP Tube", *Journal of Composites for Construction*, ASCE, 21 (5), 04017029.
[24] ASTM C39/C39M. (2011). *Standard Test Method for Compressive Strength of Cylindrical Concrete Specimens*, American Society for Testing and Materials, Philadelphia, USA.
[25] ASTM D2290-08. (2008). *Standard Test Method for Apparent Hoop Tensile Strength of Plastic or Reinforced Plastic Pipe by Split Disk Method*, American Society for Testing and Materials (ASTM), Philadelphia, USA.
[26] GB/T5350-2005. (2005). *Fiber-Reinforced Thermosetting Plastic Composites Pipe: Determination for Longitudinal Compressive Properties*, The Standards Press of China.
[27] BS 18-1987. (1987). *Tensile Testing of Metals (including Aerospace Materials*), British Standards Institution, London, UK.
[28] Lam, L., and Teng, J. G. (2009). "Stress-strain model for FRP-confined concrete under cyclic axial compression." *Engineering Structures*, 31(2), 308-321.
[29] Ramberg, W. and Osgood, W.R. (1943). "Description of stress-strain curves by three parameters", *Technical Note 902, National Advisory Committee for Aeronautics, Washington, DC.*
[30] Menegotto, M. and Pinto, P.E. (1973). "Method of analysis for cyclically loaded RC frames including changes in geometry and non-elastic behaviour of elements under combined normal force and bending", *IABSE Symposium on Resistance and Ultimate Deformability of Structures Acted on by Well-Defined Repeated Loads, Final Report, Lisbon.*
[31] Yokoo, Y. and Nakamura, T. (1977). "Non-stationary hysteretic uniaxial stress-strain relations of a wide-flange steel", *Transactions of Architectural Institute of Japan*, 260, 71-80.
[32] Mansour, M., Lee, J.Y. and Hsu, T.T. (2001). "Cyclic stress-strain curves of concrete and steel bars in membrane elements", *Journal of Structural Engineering*, ASCE, 127(12), 1402-1411.
[33] Rousakis, T. C. (2001). "Experimental Investigation of Concrete Cylinders Confined by Carbon FRP Sheets Under Monotonic and Cyclic Axial Compression Load", Research Report 01:2, Division of Building Technology, Chalmers Univ. of Technology, Gothenburg, Sweden.
[34] Ilki, A. and Kumbasar, N. (2003). "Compressive behavior of carbon fiber composite jacketed concrete with circular and non-circular cross sections." *Journal of Earthquake Engineering*, 7(3), 381–406.
[35] Lam, L., Teng, J.G., Cheung, C.H. and Xiao, Y. (2006). "FRP-confined concrete under axial cyclic compression", *Cement and Concrete Composites*, 28, 949-958.
[36] Wang, Z.Y., Wang, D.Y., Simth, S.T. and Lu, D.G. (2012). "Experimental testing and analytical modeling of CFRP-confined large circular RC columns subjected to cyclic axial compression", *Engineering Structures*, 40, 67-74.

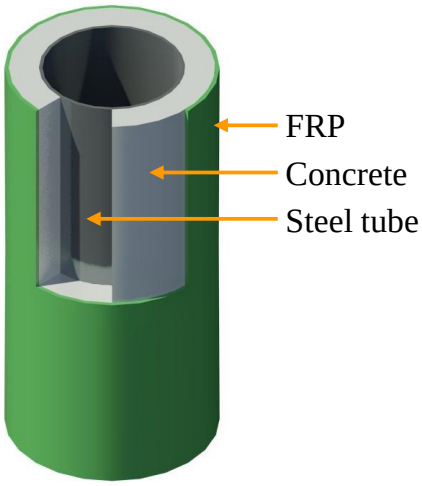

Figure 1: Hybrid DSTC

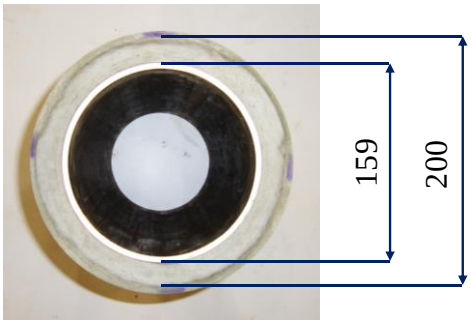

(a) Specimen with type A steel tube

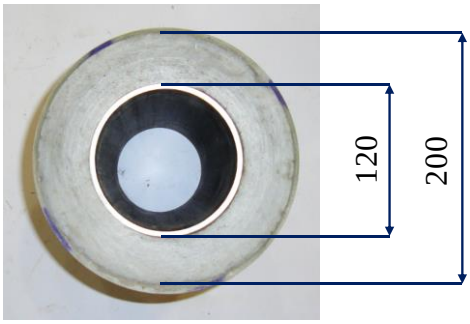

(b) Specimen with type B steel tube

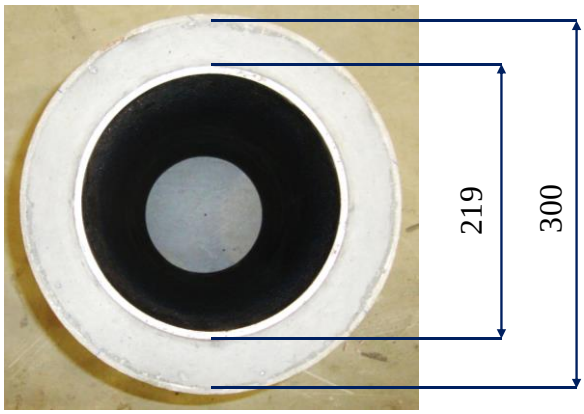

(c) Specimen with type C steel tube

Figure 2: Cross-sections of hybrid DSTC specimens (dimensions in mm)

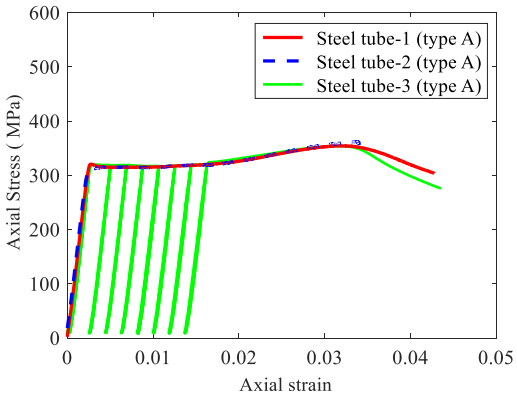

(a) Type A steel tube

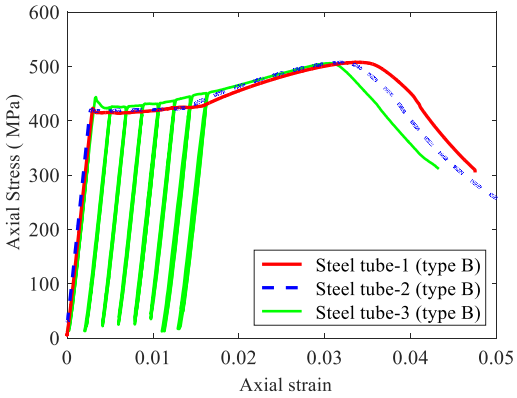

(b) Type B steel tube

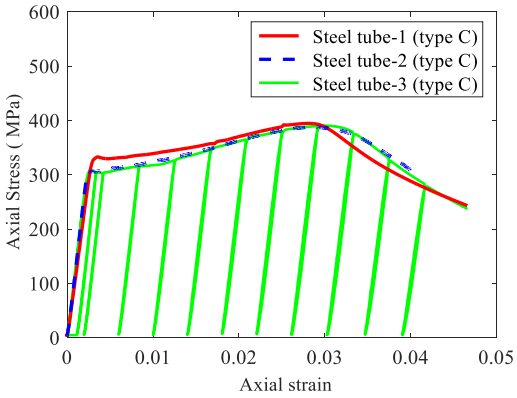

(c) Type C steel tube

Figure 3: Axial stress-axial strain curves of steel tubes

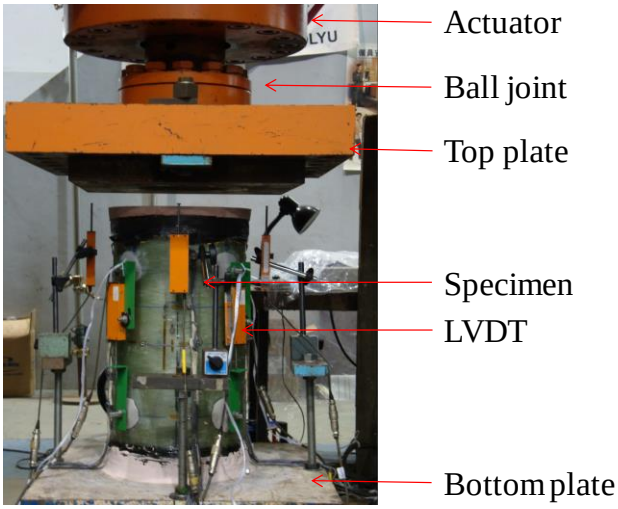

Figure 4: Experimental setup

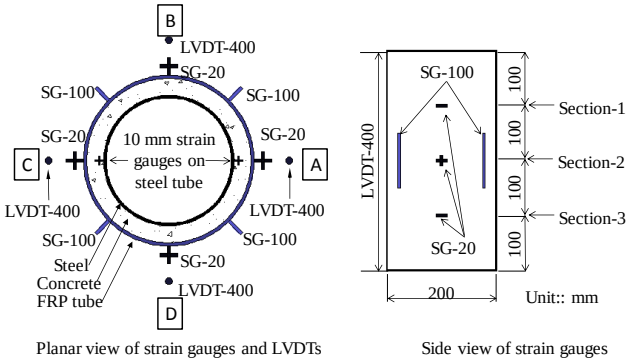

(a) Specimens of batches 1-3

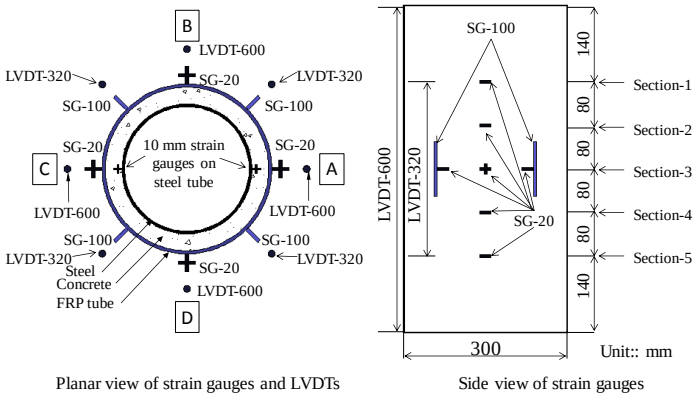

(b) Specimens of batches 4-6

Figure 5: Layout of strain gauges and LVDTs

(a) D54-2FW-C

(b) D104-4FW-C

(c) D40-6FW-C1

(d) D85-6FW-C2

Figure 6: Typical specimens after test

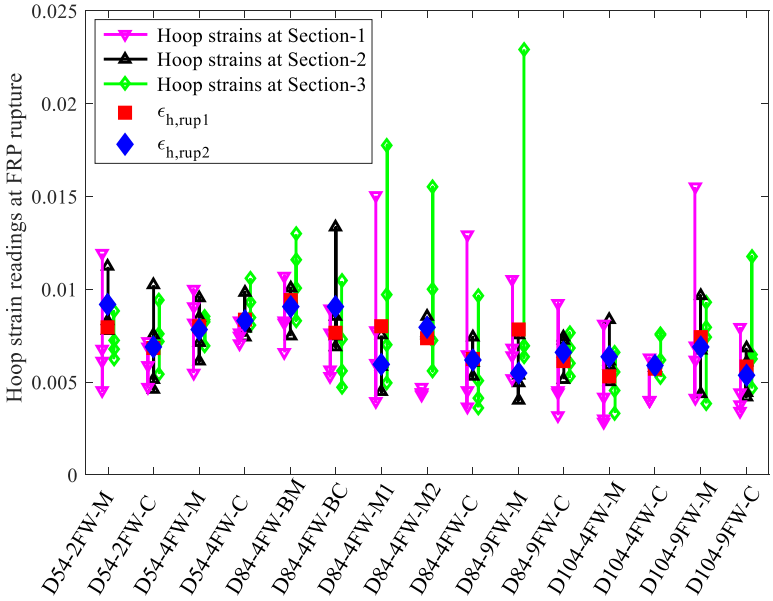

(a) Specimens of batches 1-3

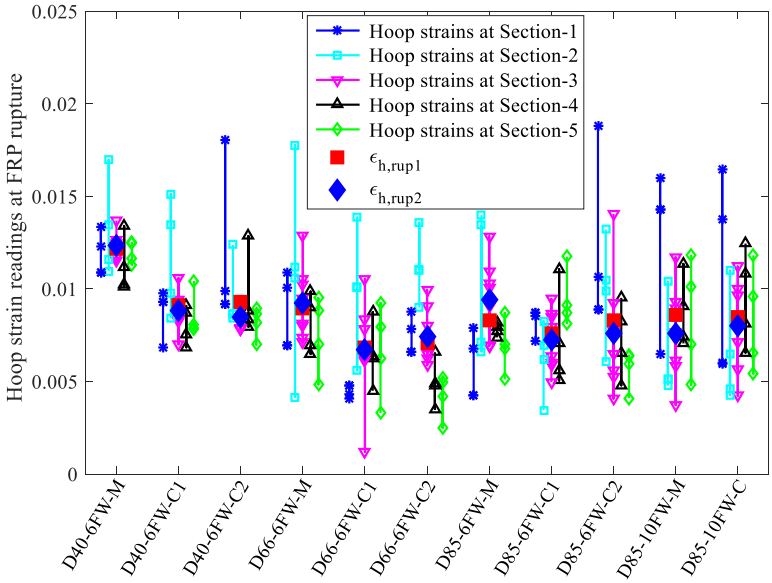

(b) Specimens of batches 4-6

Figure 7: Hoop strain distributions

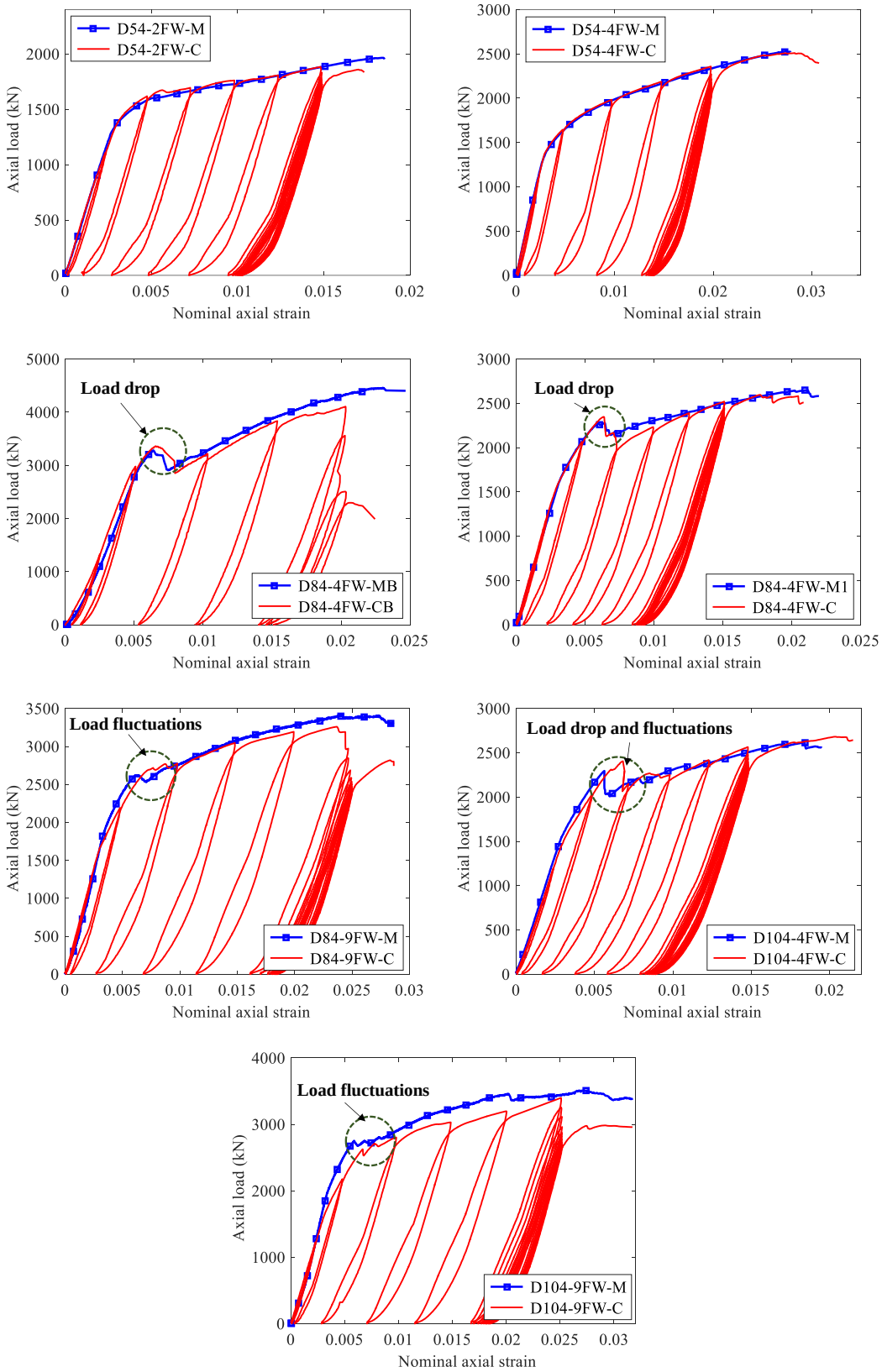

(a) Specimens of batches 1-3

Figure 8: Axial load-axial strain curves of typical hybrid DSTCs

(to be continued)

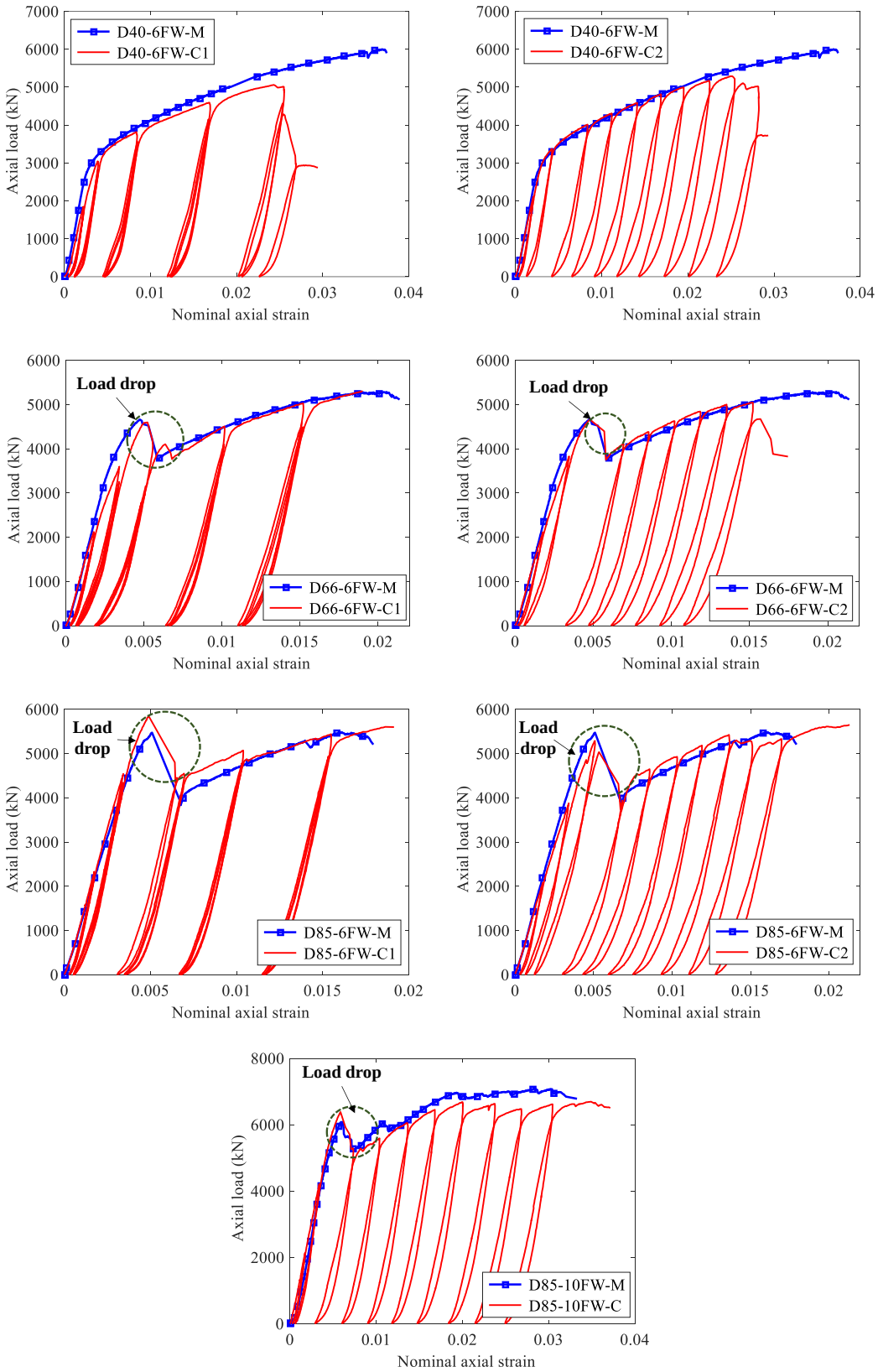

(b) Specimens of batches 4-6

Figure 8: Axial load-axial strain curves of typical hybrid DSTCs

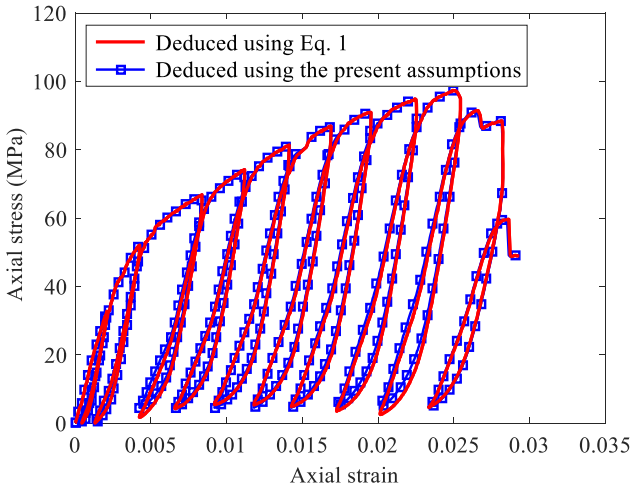

(a) D40-6FW-C2

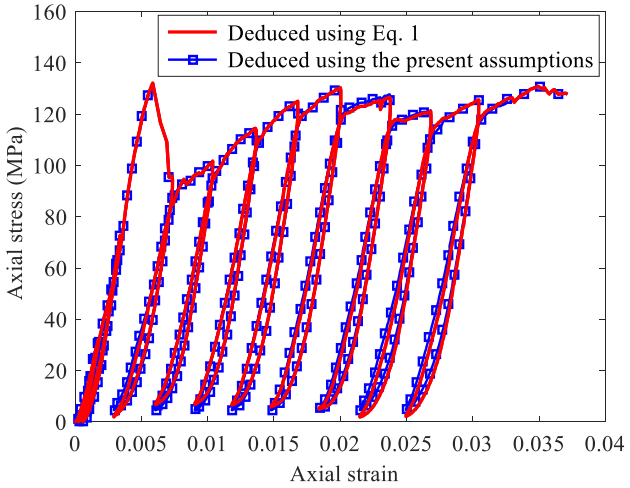

(b) D85-10FW-C

Figure 9: Cyclic axial stress-strain curves of concrete obtained using two different methods

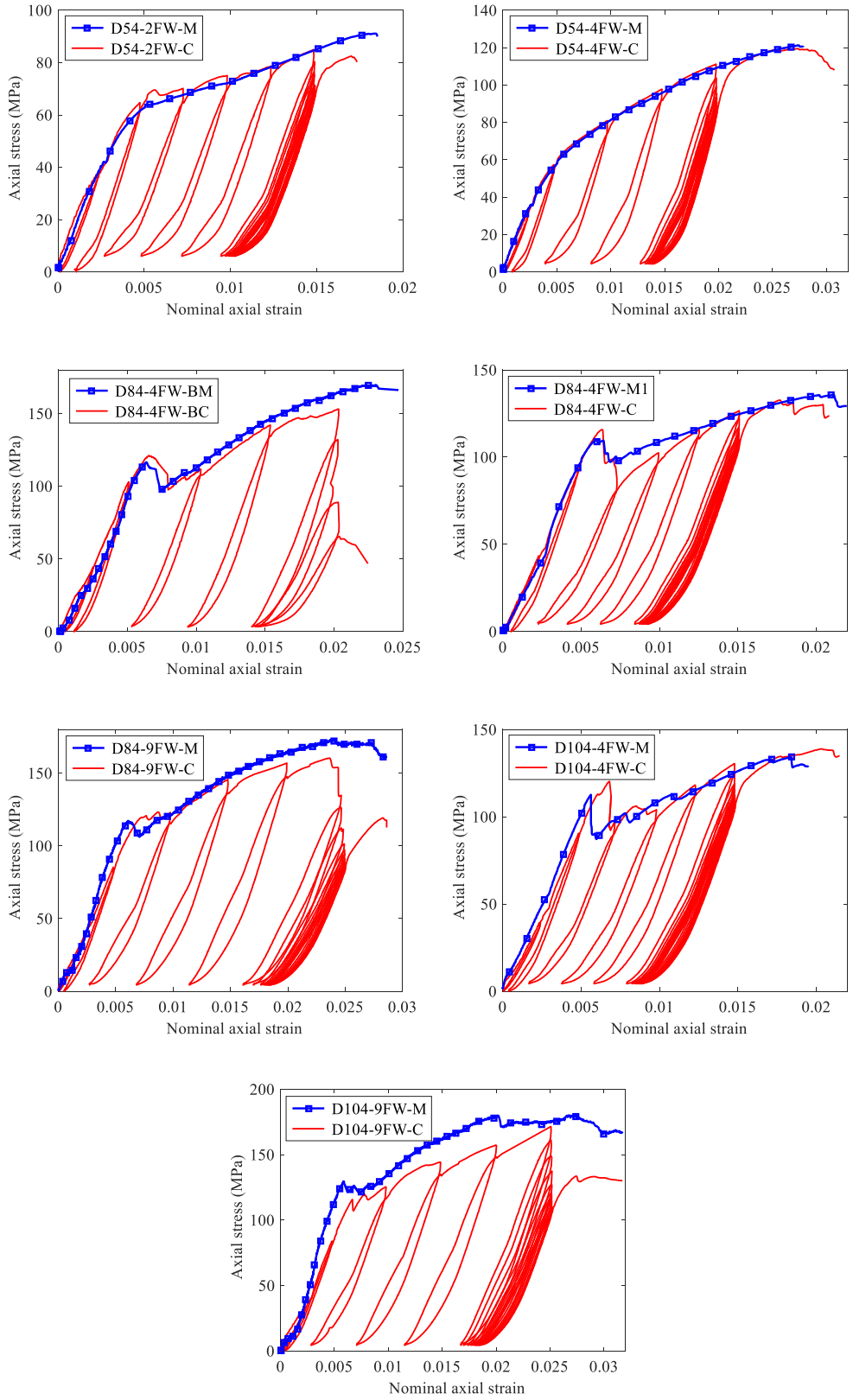

(a) Specimens of batches 1-3

Figure 10: Cyclic axial stress-strain curves of concrete

(to be continued)

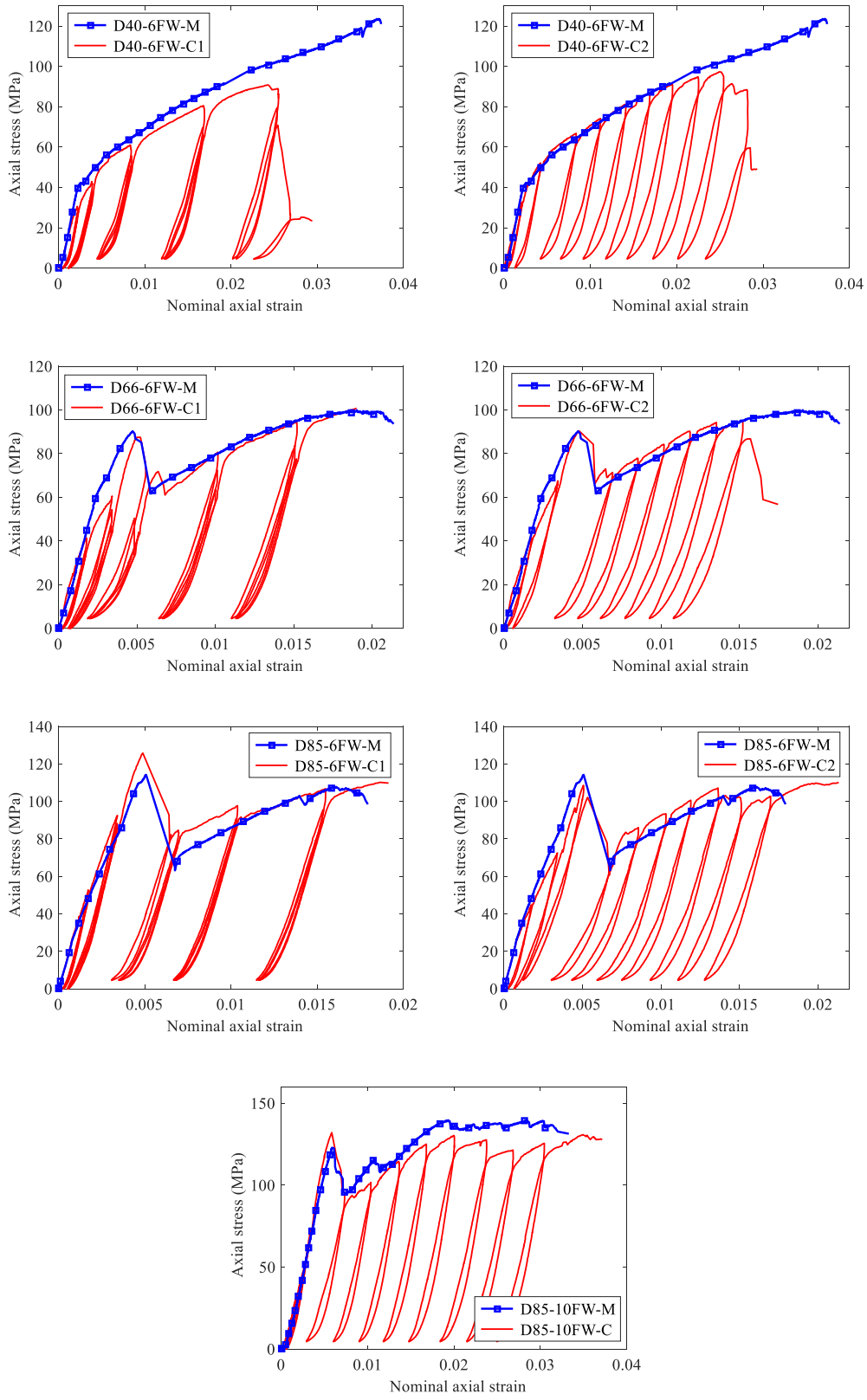

(b) Specimens of batches 4-6

Figure 10: Cyclic axial stress-strain curves of concrete

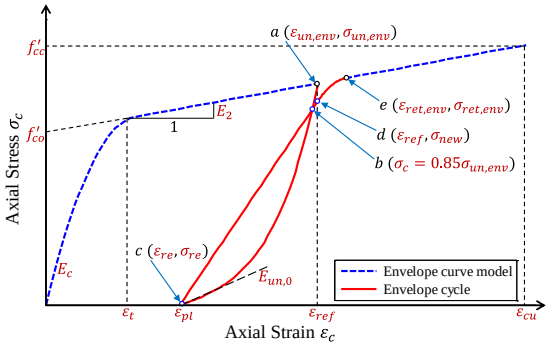

$\boldsymbol{\varepsilon_{cu}}$ and $\boldsymbol{f'_{cc}}$: ultimate strain and ultimate stress of confined concrete
$\boldsymbol{\varepsilon_{un,env}}$ and $\boldsymbol{\sigma_{un,env}}$: envelope unloading strain and envelope unloading stress
$\boldsymbol{\varepsilon_{re}}$ and $\boldsymbol{\sigma_{re}}$: reloading strain and reloading stress on the reloading curve
$\boldsymbol{\varepsilon_{ref}}$ and $\boldsymbol{\sigma_{new}}$: reference strain and new stress on the reloading curve
$\boldsymbol{\varepsilon_{ret,env}}$ and $\boldsymbol{\sigma_{ret,env}}$: return strain and return stress on the reloading curve
$\boldsymbol{E_c}$: initial Young's Modulus of confined concrete
$\boldsymbol{E_2}$: slope of the second branch
$\boldsymbol{E_{un,0}}$: slope of the unloading curve when the unloading stress is zero
$\boldsymbol{\varepsilon_t}$: transition strain between the parabola portion and the linear portion
$\boldsymbol{\varepsilon_{pl}}$: plastic strain of the envelope curve

(a) Envelope cycle

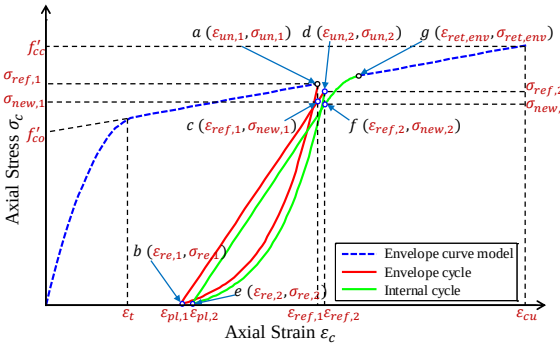

$\boldsymbol{\varepsilon_{un,1}}$ and $\boldsymbol{\sigma_{un,1}}$: envelope unloading strain and envelope unloading stress
$\boldsymbol{\varepsilon_{un,2}}$ and $\boldsymbol{\sigma_{un,2}}$: second unloading strain and second unloading stress
$\boldsymbol{\varepsilon_{re,1}}$ and $\boldsymbol{\sigma_{re,1}}$: first reloading strain and first reloading stress
$\boldsymbol{\varepsilon_{re,2}}$ and $\boldsymbol{\sigma_{re,2}}$: second reloading strain and second reloading stress
$\boldsymbol{\varepsilon_{ref,1}}$ and $\boldsymbol{\sigma_{new,1}}$: first reference strain and first new stress
$\boldsymbol{\varepsilon_{ref,2}}$ and $\boldsymbol{\sigma_{new,2}}$: second reference strain and second new stress
$\boldsymbol{\varepsilon_{ret,env}}$ and $\boldsymbol{\sigma_{ret,env}}$: return strain and return stress on the reloading curve
$\boldsymbol{\varepsilon_{pl,1}}$: plastic strain of the first unloading curve
$\boldsymbol{\varepsilon_{pl,2}}$: plastic strain of the second unloading curve

(b) Internal cycles

Figure 11: Key parameters of cyclic stress-strain curves of FRP-confined concrete

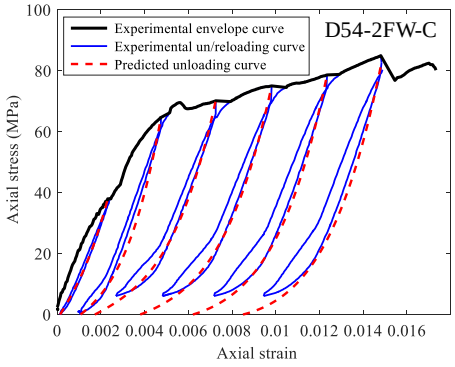

(a) D54-2FW-C

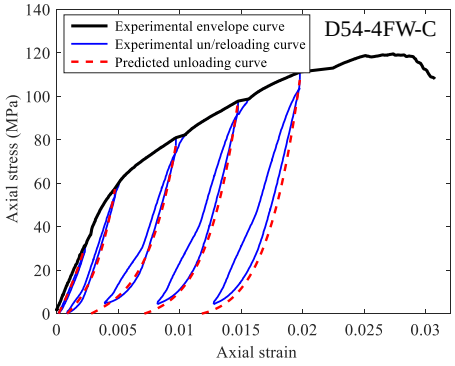

(b) D54-4FW-C

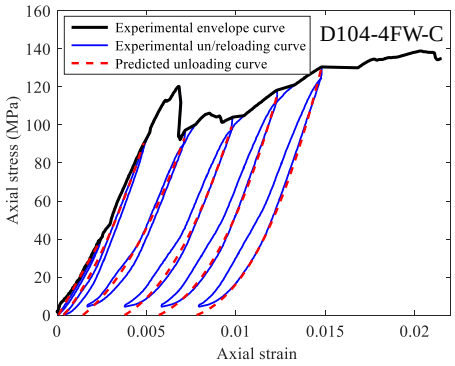

(c) D104-4FW-C

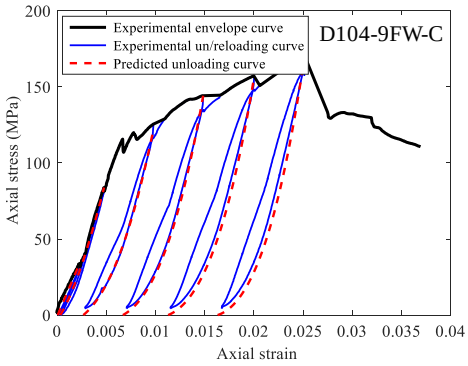

(d) D104-9FW-C

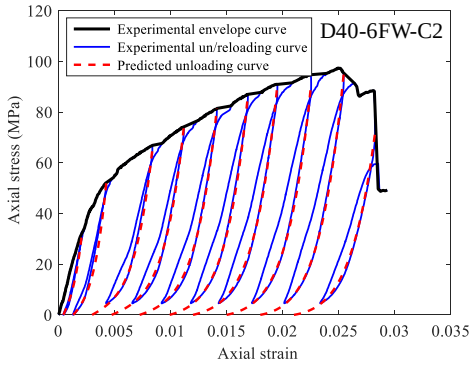

(e) D40-6FW-C2

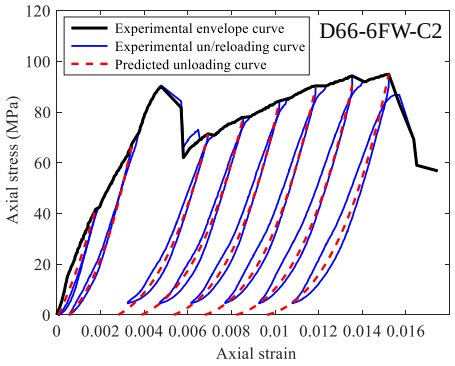

(f) D66-6FW-C2

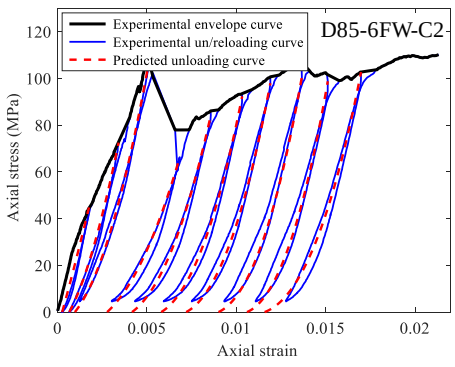

(g) D85-6FW-C2

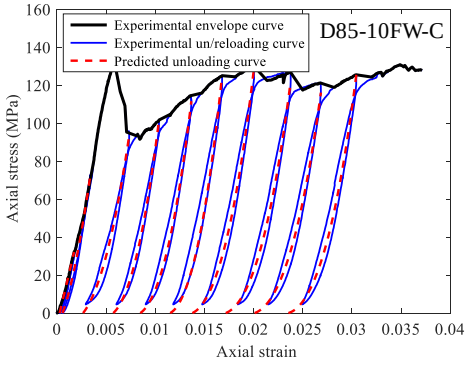

(h) D85-10FW-C

Figure 12: Prediction of unloading curves

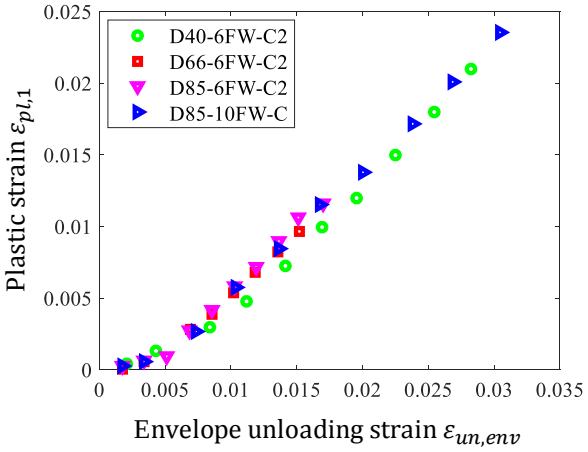

(a) Specimens of batches 1-3

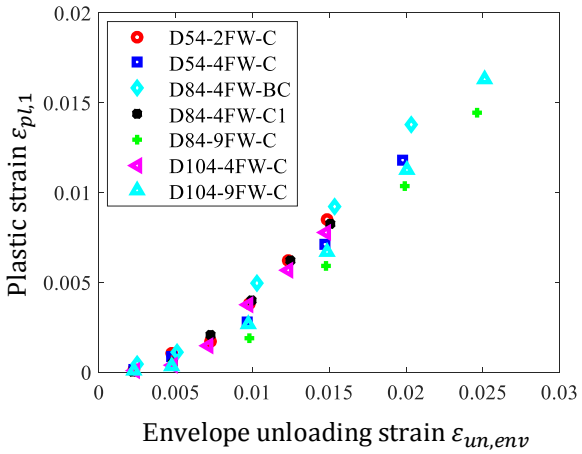

(b) Specimens of batches 4-6

Figure 13: Relationship between plastic strains and envelope unloading strains

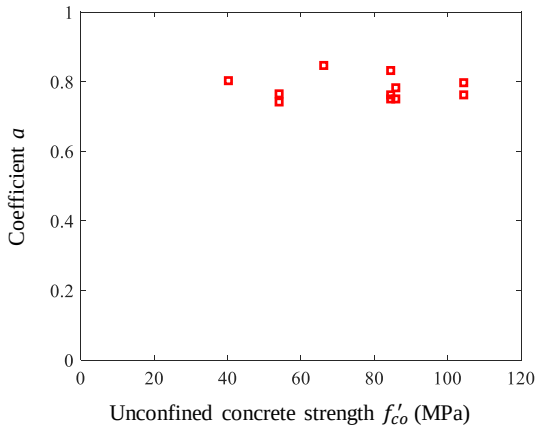

Figure 14: Effect of concrete strength on the plastic strain

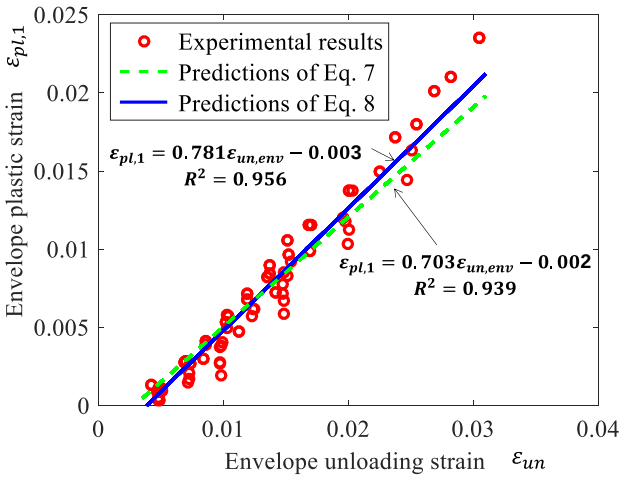

Figure 15: Performance of equations for the plastic strain of envelope cycles

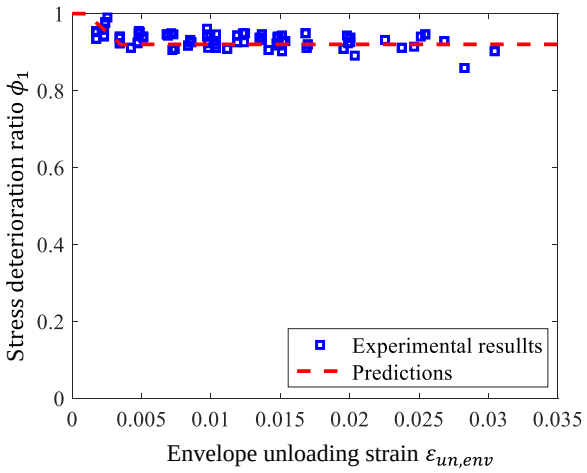

Figure 16: Performance of equations for the stress deterioration ratio of envelope cycles

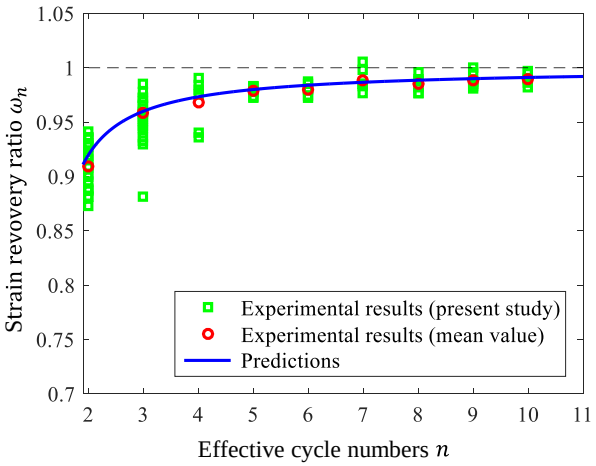

Figure 17: Performance of equations for the strain recovery ratio of internal cycles

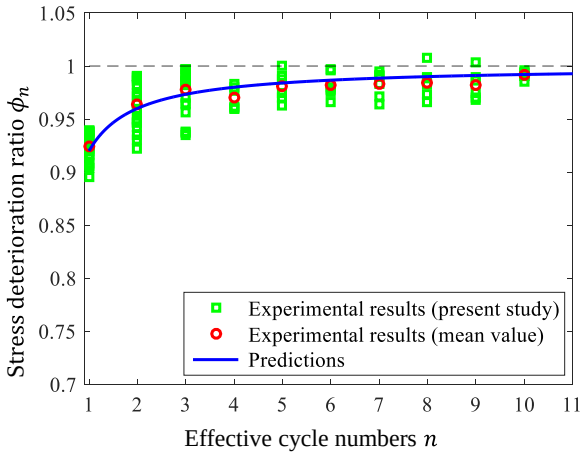

Figure 18: Performance of equations for the stress deterioration ratio of internal cycles

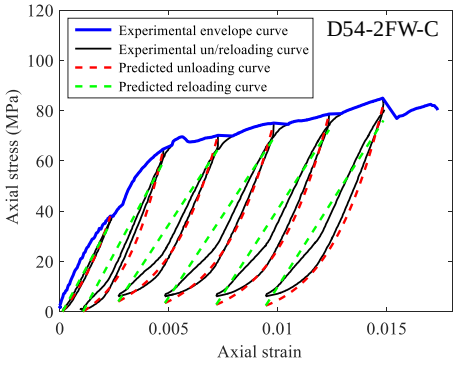

(a) D54-2FW-C

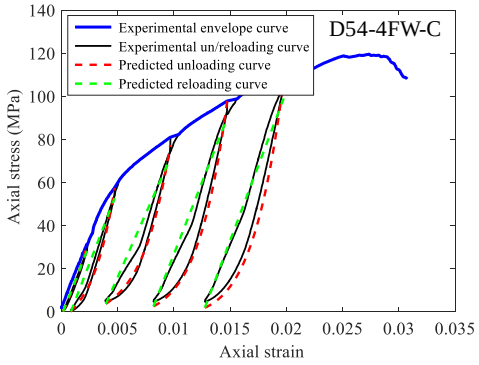

(b) D54-4FW-C

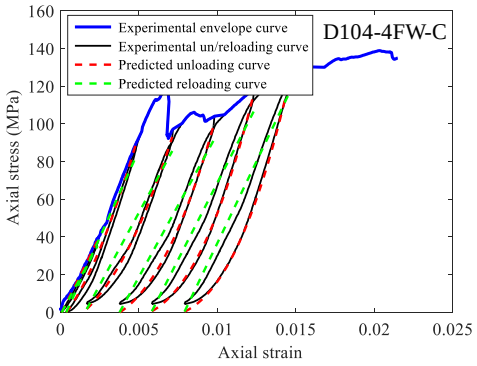

(c) D104-4FW-C

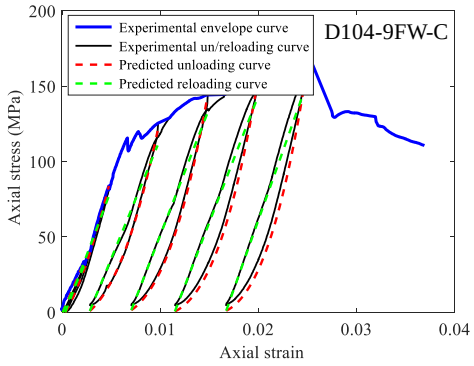

(d) D104-9FW-C

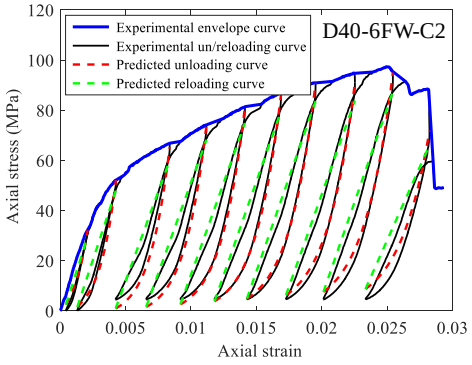

(e) D40-6FW-C2

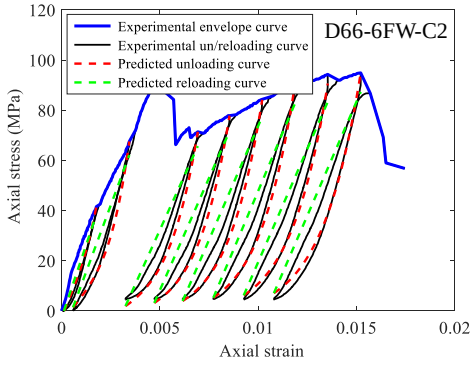

(f) D66-6FW-C2

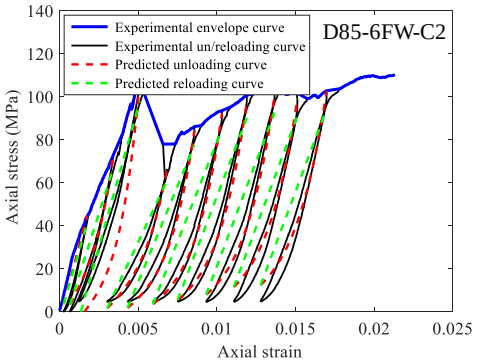

(g) D85-6FW-C2

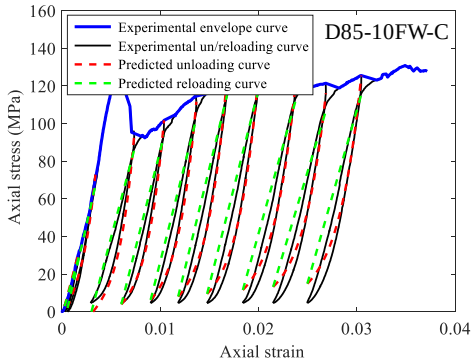

(h) D85-10FW-C

Figure 19: Performance of equations for envelope unloading/reloading curves

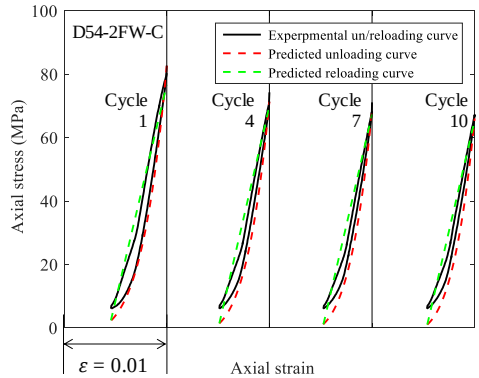

(a) D54-2FW-C

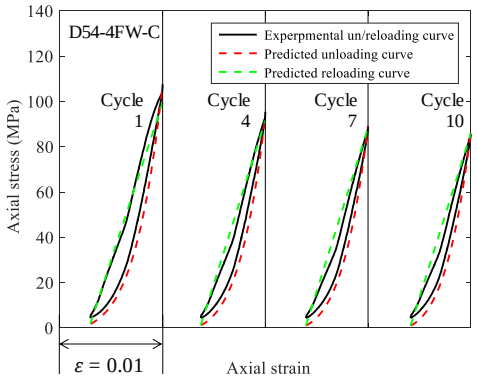

(b) D54-4FW-C

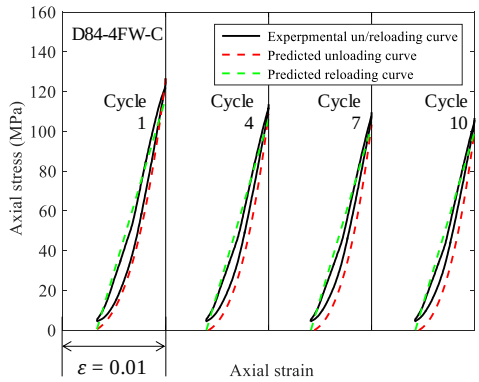

(c) D84-4FW-C

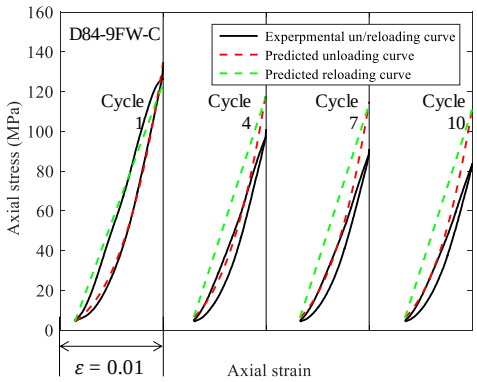

(d) D84-9FW-C

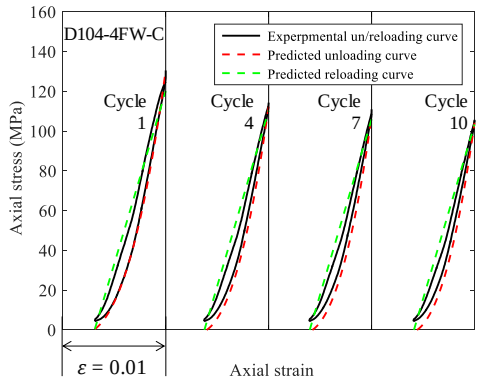

(e) D104-4FW-C

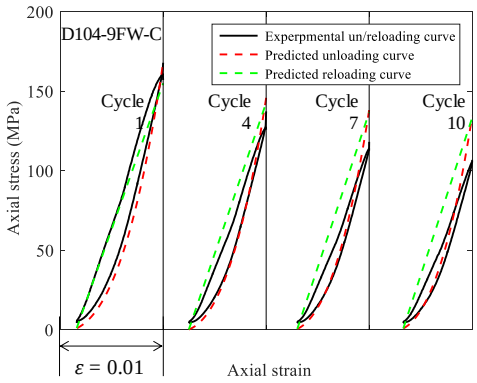

(f) D104-9FW-C

Figure 20: Performance of equations for repeated unloading/reloading curves

Table 1: Details of DSTC specimens

Specimen	Specimen dimensions			Steel tube		FRP tube		Concrete batch
	Diameter (mm)	Height (mm)	φ	Type	D_s/t_s	Type	t_{frp} (mm)	
D54-2FW-M	200	400	0.795	A	31.8	2FW	2.2	1 (54.1MPa)
D54-2FW-C	200	400	0.795	A	31.8	2FW	2.2	
D54-4FW-M	200	400	0.795	A	31.8	4FW	4.7	
D54-4FW-C	200	400	0.795	A	31.8	4FW	4.7	
D84-4FW-M1	200	400	0.795	A	31.8	4FW	4.7	2 (84.6MPa)
D84-4FW-M2	200	400	0.795	A	31.8	4FW	4.7	
D84-4FW-C	200	400	0.795	A	31.8	4FW	4.7	
D84-4FW-MB	200	400	0.600	B	26.7	4FW	4.7	
D84-4FW-CB	200	400	0.600	B	26.7	4FW	4.7	
D84-9FW-M	200	400	0.795	A	31.8	9FW	9.5	
D84-9FW-C	200	400	0.795	A	31.8	9FW	9.5	
D104-4FW-M	200	400	0.795	A	31.8	4FW	4.7	3 (104.4MPa)
D104-4FW-C	200	400	0.795	A	31.8	4FW	4.7	
D104-9FW-M	200	400	0.795	A	31.8	9FW	9.5	
D104-9FW-C	200	400	0.795	A	31.8	9FW	9.5	
D40-6FW-M	300	600	0.730	C	36.5	6FW	6.0	4 (40.9MPa)
D40-6FW-C1	300	600	0.730	C	36.5	6FW	6.0	
D40-6FW-C2	300	600	0.730	C	36.5	6FW	6.0	
D66-6FW-M	300	600	0.730	C	36.5	6FW	6.0	5 (66.1MPa)
D66-6FW-C1	300	600	0.730	C	36.5	6FW	6.0	
D66-6FW-C2	300	600	0.730	C	36.5	6FW	6.0	
D85-6FW-M	300	600	0.730	C	36.5	6FW	6.0	6 (85.8MPa)
D85-6FW-C1	300	600	0.730	C	36.5	6FW	6.0	
D85-6FW-C2	300	600	0.730	C	36.5	6FW	6.0	
D85-10FW-M	300	600	0.730	C	36.5	10FW	10.0	
D85-10FW-C	300	600	0.730	C	36.5	10FW	10.0	

Table 2: Dimensions and properties of steel tubes

Type	D_s (mm)	t_s (mm)	Elastic modulus E_s (GPa)	Yield stress f_y (MPa)	Ultimate stress f_u (MPa)
A	159	5.0	205.8	320.4	512.3
B	120	4.5	199.6	419.5	565.7
C	219	6.0	198.7	319.4	441.5

Table 3: Mix proportions of concrete

Specimen batch	Water-cement ratio	Water	Cement	Fly ash	Silica fume	Super plasticizer*	Coarse aggregate	Sand
		(kg/m^3)						
1	0.35	175	300	200	---	9	829	796
2	0.29	174	377	203	29	11	793	762
3	0.23	155	442	170	68	16	819	712
4	0.42	186	239	203	---	3	822	715
5	0.35	175	300	200	---	10	845	812
6	0.30	174	377	203	29	11	793	762

*The brand of the super plasticizer is "Grace HK", and the product model is "ADVA109".

Table 4: Properties of concrete

Batch No.	f_{co} (MPa)	E_c (GPa)	ε_{co} (%)
1	54.1	27.8	0.26
2	84.6	33.1	0.27
3	104.4	36.4	0.31
4	40.9	23.5	0.22
5	66.1	30.0	0.25
6	85.8	33.9	0.27

Table 5: Cyclic loading schemes

Specimen	Unloading displacement (mm)									
	Step 1	Step 2	Step 3	Step 4	Step 5	Step 6	Step 7	Step 8	Step 9	Step 10
D54-2FW-C	0.92	1.90	2.90	3.93	4.94	5.94/10*	---	---	---	---
D54-4FW-C	0.91	1.89	3.87	5.90	7.90/10*	---	---	---	---	---
D84-4FW-CB	1.00	2.04	4.13	6.15	8.13/3*	---	---	---	---	---
D84-4FW-C	0.89	1.92	2.91	3.98	5.00	6.03/10*	---	---	---	---
D84-9FW-C	0.94	1.92	3.91	5.92	7.96	9.86/10*	---	---	---	---
D104-4FW-C	0.95	1.94	2.85	3.90	4.92	5.91/10*	---	---	---	---
D104-9FW-C	0.92	1.91	3.90	5.94	8.01	10.0/10*	---	---	---	---
D40-6FW-C1	1.34/3*	2.36/3*	5.07/3*	10.1/3*	15.3/3*	---	---	---	---	---
D40-6FW-C2	1.26	2.56	5.03	6.71	8.48	10.14	11.7	13.5	15.2	16.9
D66-6FW-C1	1.08/3*	2.05/3*	3.34/3*	6.10/3*	9.13/3*	---	---	---	---	---
D66-6FW-C2	1.06	2.07	2.87	5.12	6.12	7.12	8.12	9.13		---
D85-6FW-C1	1.04/3*	2.05/3*	3.91/3*	6.23/3*	9.29/3*	---	---	---	---	---
D85-6FW-C2	1.05	2.05	3.05	4.10	5.14	6.20	7.14	8.20	9.07	10.1
D85-10FW-C	1.05	2.04	4.41	6.23	8.20	10.0	12.0	14.2	16.1	18.2

* The number after the back slash is the number of repeated cycles at the prescribed unloading displacement; for those without this number, a single unloading/reloading cycle was applied.

Table 6: Key test results of DSTC specimens

Specimen	F_{all} (kN)	F_c (kN)	f'_{cc} (MPa)	ε_{cu} (%)	$\frac{f'_{cc}}{f'_{co}}$	$\frac{\varepsilon_{cu}}{\varepsilon_{co}}$	$\varepsilon_{h,rup1}$ (%)	$\varepsilon_{h,rup2}$ (%)
D54-2FW-M	1965	1053	91.1	1.85	1.69	7.19	0.79	0.92
D54-2FW-C	1885	982	85.0	1.73	1.57	6.73	0.68	0.69
D54-4FW-M	2530	1401	121.2	2.79	2.25	10.7	0.80	0.78
D54-4FW-C	2509	1381	119.5	3.07	2.21	11.9	0.83	0.83
D84-4FW-MB	4461	3410	169.7	2.47	2.01	8.98	0.94	0.91
D84-4FW-CB	4106	3077	153.1	2.25	1.81	8.17	0.77	0.91
D84-4FW-M1	2650	1567	135.6	2.20	1.60	8.15	0.80	0.60
D84-4FW-M2	2763	1683	145.7	2.30	1.72	8.52	0.73	0.79
D84-4FW-C	2597	1533	132.7	2.08	1.57	7.58	0.62	0.62
D84-9FW-M	3413	2005	173.5	2.86	2.05	10.6	0.78	0.55
D84-9FW-C	3260	1853	160.4	2.86	1.90	10.6	0.61	0.66
D104-4FW-M	2616	1550	134.2	1.95	1.29	6.26	0.53	0.64
D104-4FW-C	2682	1605	138.9	2.15	1.33	6.90	0.57	0.59
D104-9FW-M	3512	2082	180.2	3.17	1.73	10.2	0.74	0.69
D104-9FW-C	3400	1982	171.5	3.17	1.64	10.2	0.59	0.54
D40-6FW-M	6002	4079	123.6	3.74	3.02	16.9	1.23	1.20
D40-6FW-C1	5059	2998	90.8	2.94	2.22	13.3	0.92	0.88
D40-6FW-C2	5290	3213	97.4	2.93	2.38	13.2	0.93	0.85
D66-6FW-M	5284	3299	100.0	2.14	1.51	8.50	0.93	0.95
D66-6FW-C1	5304	3326	100.8	1.90	1.52	7.56	0.69	0.65
D66-6FW-C2	5045	3131	94.9	1.75	1.44	6.94	0.70	0.72
D85-6FW-M	5482	3771	114.3	1.79	1.33	6.68	0.83	0.91
D85-6FW-C1	5846	4154	125.9	1.91	1.47	7.13	0.77	0.73
D85-6FW-C2	5651	3637	110.2	2.13	1.28	7.94	0.83	0.78
D85-10FW-M	7089	4610	139.7	3.33	1.62	12.4	0.85	0.80
D85-10FW-C	6695	4360	132.1	3.71	1.53	13.8	0.85	0.80

Table 7: Regression analysis for plastic strains

Specimen	Unconfined concrete strength f'_{co} (MPa)	$\varepsilon_{pl,1} = a\varepsilon_{un,env} + b$		R^2
		a	b	
D54-2FW-C	54.1	0.766	-0.0032	0.970
D54-4FW-C	54.1	0.742	-0.0034	0.972
D84-4FW-CB	84.6	0.831	-0.0032	0.997
D84-4FW-C	84.6	0.762	-0.0034	0.997
D84-9FW-C	84.6	0.750	-0.0032	0.975
D104-4FW-C	104.4	0.763	-0.0032	0.993
D104-9FW-C	104.4	0.797	-0.0034	0.985
D40-6FW-C2	40.1	0.802	-0.0027	0.991
D66-6FW-C2	66.1	0.846	-0.0032	0.985
D85-6FW-C2	85.8	0.752	-0.0020	0.993
D85-10FW-C	85.8	0.782	-0.0025	0.995